A Path/Surface Following Control Approach to Generate Virtual Fixtures

authored by **B. Bischof, T. Glück, M. Böck, and A. Kugi**

and published in *IEEE Transactions on Robotics*.


```
@Article{acinpaper,
  author = {Bischof, B. and Gl\"uck, T. and B\"ock, M. and Kugi, A.},
  title = {A Path/Surface Following Control Approach to Generate Virtual Fixtures},
  journal = {IEEE Transactions on Robotics},
  year = {2018},
  volume = {34},
  number = {6},
  pages = {1577--1592},
  issn = {1552-3098},
  doi = {10.1109/TRO.2018.2861913},
  timestamp = {2019-01-09},
}
```


Automation and Control Institute (ACIN)
TU Wien
Gusshausstrasse 27-29/E376
1040 Vienna, Austria

Internet: www.acin.tuwien.ac.at
E-mail: office@acin.tuwien.ac.at
Phone: +43 1 58801 37601
Fax: +43 1 58801 37699

A Path/Surface Following Control Approach to Generate Virtual Fixtures

Bernhard Bischof, Tobias Glück, Martin Böck, and Andreas Kugi, *Member, IEEE*

***Abstract*—The workspace of a robot can be restricted by virtual fixtures to assist an operator in physical human-robot interaction tasks. This paper introduces a combination of surface following control with compliance control and presents a path/surface following control approach to systematically generate virtual fixtures. This approach allows to implement numerous types of constraints like guidance and forbidden region virtual fixtures, hard and soft constraints as well as static and dynamic virtual fixtures and their combinations. Additionally, closed-loop stability proofs of the proposed control concepts are given. The flexibility of the presented approach is demonstrated by a series of measurement results from an industrial robot.**

***Index Terms*—Virtual Fixture, Active Constraints, Physical Human-Robot Interaction, Surface Following Control, Path Following Control, Compliance Control.**

I. Introduction

VIRTUAL fixtures restrict the workspace of a manipulator by means of control algorithms. With these approaches the safety of an operator in semi-automated production using hand-guided physical human-robot interaction can be increased [1], [2]. Additionally, virtual fixtures help to guide the operator and, thus, can speed up the production process as well as reduce the worker's risk for repeated trauma disorders [3], [4]. Virtual fixtures are used in the automotive industry since the late 1990s [5]. They are also common in teleoperation and hand-guided operation in robotically assisted surgery [2], [6].

On the basis of [7], we identified six principal methods to generate virtual fixtures (often also denoted as active constraints) in literature; these are (i.) simple functions of constraint proximity, (ii.) potential fields, (iii.) non-energy storing constraints, (iv.) constrained joint optimization, (v.) reference direction fixtures, and (vi.) passive constraint enforcing mechanisms. The virtual fixtures can either be guidance constraints, where the motion is restricted to a specific manifold like a path, or forbidden-region constraints, where the motion is free unless a forbidden region is entered [2]. In both cases, the constraints can be soft or hard. Soft constraints allow some deviation while hard constraints limit the motion to the virtual fixture.

(i.) Guidance constraints [8] and forbidden-region constraints [9] can be generated by simple functions of constraint proximity. Only soft constraints can be achieved within this approach, because the constraint force vector is a linear function of the closest distance to the constraint manifold effectively emulating a spring. In [9], Abbot and Okamura investigated the stability of the control law for a linear system, where the human operator is modeled as a linear and time-invariant mass-spring-damper system. They concluded that the stability of the closed-loop system decreases with an increasing stiffness of the constraint and the constraint cannot be made arbitrarily stiff.

(ii.) Potential fields can also be used to establish virtual fixtures, where areas in the workspace with low potential are attractive and areas with high potential are repulsive. In [10], the potential field approach was employed to generate forbidden-region constraints for collision avoidance. At each point in the workspace, the gradient of the potential field of all sources has to be calculated to determine the resulting force that pulls the robot away from the forbidden regions. Also guidance constraints can be generated using attractive fields resulting in a control law very similar to the method of simple functions described above.

(iii.) A non-energy storing constraint was introduced in [11] by using simulated plasticity, which is modeled as Coulomb friction. The initial collision with the constraint is thereby stiff until a certain force into the restricted area is applied. When penetrating the constraint, energy is only dissipated and no energy is stored. Hence, no force is applied by the control law to recover the penetration. According to the authors, the non-energy storing feature can increase the safety for various applications. Some effort was made to deal with the discontinuity of the plasticity. A virtual proxy is introduced on which the plasticity takes effect. The proxy is then coupled to the haptic device or manipulator via a spring and a damper. This reduces the discontinuity problem but adds some (small) stored potential energy. Bowyer and F. y Baena improved this approach significantly in [12]. Friction redirection was introduced to assist the operator in recovering from penetrations of the constraint. Additionally, their approach allows for time-variant constraints and they showed that their control law is dissipative even for combined translational and rotational constraints.

(iv.) Constrained joint optimization is used since the early nineties to establish virtual fixtures for surgical robots, which can also be redundant [6]. A constrained optimization problem is solved to compute the new refer-

B. Bischof, M. Böck, and A. Kugi are with the Automation and Control Institute, TU Wien, 1040 Vienna, Austria, e-mail: {bischof,boeck,kugi}@acin.tuwien.ac.at, T. Glück is with the AIT Austrian Institute of Technology, Center for Vision, Automation & Control, 1040 Vienna, Austria, e-mail: tobias.glueck@ait.ac.at.

Post-print version of the article: B. Bischof, T. Glück, M. Böck, and A. Kugi, "A path/surface following control approach to generate virtual fixtures", *IEEE Transactions on Robotics*, vol. 34, no. 6, pp. 1577–1592, 2018, ISSN: 1552-3098. DOI: 10.1109/TRO.2018.2861913
The content of this post-print version is identical to the published paper but without the publisher's final layout or copy editing.

ence velocities of the joints at each sampling instance. A cost function is minimized that represents the difference between reference velocities given from the operator and new reference velocities satisfying the constraints. The constraints can include the virtual fixtures as well as mechanical and dynamic limits of the joints. Linear constraints for point fixtures are given in [6]. They are extended to line and plane fixtures in [13]. With this method, the constraints are probably not satisfied in between the sampling instants. Therefore, the sampling intervals have to be relatively short compared to the maximum velocity of the manipulator. To find optimal solutions that fulfill nonlinear constraints can be a challenging task. Hence, the numerical implementation has to be carried out very carefully for each application to ensure an appropriate and stable behavior.

(v.) In [14], reference direction fixtures were introduced to establish constrained hand-guided operation. The input force of an operator is thereby projected onto the tangential direction or onto the tangential plane of the constraint manifold and is used as velocity reference for the servo controllers. This restricts the motion of the robot parallel to the manifold. The constraint can be made soft by adding a fraction of the operators force orthogonal to the manifold in the control law. When the robot is off the manifold, the direction of the force projection is modified to guide the operator towards the manifold. A stability analysis is carried out for the simple case of a linear two-dimensional manipulator. However, even in this case, stability can only be proven when the robot is exactly on the manifold. Castillo-Cruces and Wahrburg [15] added a proportional error term in the control law to make the manifold attractive and also extended the algorithm to six degrees of freedom.

(vi.) In passive constraint enforcing mechanisms, the actuation force is applied by a human operator and the control architecture is only able to limit or redirect the motion. Therefore, these mechanisms are naturally safer than actively driven methods but their applicability is very limited and they are not suitable for teleoperation. An algorithm to achieve hard guidance constraints on a curve for wheeled passive robots was introduced in [16]. This concept was extended to active manipulators in [1] using continuously variable transmissions (CVT). With these CVTs the ratios of the angular velocities of the manipulator's joints are controlled such that only one degree of freedom is left for the end-effector that satisfies the guidance constraints. However, the control law is not defined for zero velocity and becomes ill-conditioned when the velocity is orthogonal to the curve.

In [17], path following control (PFC) is combined with compliance control for fully actuated rigid body manipulators, where the system output is stabilized on a path (one dimensional manifold) without a priori time parametrization. The approach is extended to elastic joint robots in [18]. First preliminary results of the stabilization of a two-dimensional manifold using so called surface following control (SFC) is presented in [19], which is not suitable for a combination with compliance control. Note that there also exist extensions for PFC to redundant manipulators [20].

In this paper, we improve the SFC approach of [19] such that it can be combined with compliance control. In addition, we show that a large number of virtual fixtures can be systematically generated by a combination of SFC/PFC with compliance control; i.e., guidance or forbidden-region virtual fixtures that can either be soft or hard and the constraints can also be time variant. The behavior along and away from the virtual fixtures can, thereby, be defined in a physically interpretable manner. The paths for PFC and the surfaces for SFC can be defined in terms of parametrized functions, e.g., 1D and 2D splines, which allows to approximate the geometry of the constraints. Additionally, in contrast to the approaches mentioned before, the SFC/PFC approach allows to systematically prove closed-loop stability. SFC and PFC stabilize the system's output on a predefined path or surface without a priori time parametrization. Via static state feedback, the dynamics in tangential and orthogonal directions to a path or surface are decoupled and exactly linearized. The decoupled dynamics can be controlled independently to meet the requirements of the specific application.

The combination with compliance control enables to define a virtual mass-spring-damper behavior of the robot independently in tangential and orthogonal direction to the path or surface. In hand-guided tasks, this mass-spring-damper behavior is felt by the operator when handling the robot and additionally increases the safety due to its passivity.

The paper is organized as follows. Section II introduces the combined surface following and compliance control for fully actuated manipulators. In addition, a simplified SFC approach is presented, where subordinate joint velocity controllers are used. Section III explains how and which virtual fixtures can be generated on the basis of the SFC approaches presented in Section II and of the PFC approaches summarized in Appendix A. In Section IV, an experiment on a six-axis industrial robot is performed to validate the combined surface following and compliance control. Four implementation examples to generate various virtual fixtures are presented in Section V.

II. Manifold Stabilization Method

Manifold stabilization generalizes the classical control task of set-point stabilization and aims at stabilizing submanifolds like paths and surfaces typically in the output space of a dynamic system [21], [22]. The control objectives of manifold stabilization are that the system's output asymptotically converges to and then remains on the submanifold as well as that the motion on the submanifold meets application-specific requirements. The most common form is the path following control (PFC), where a one-dimensional submanifold of the output space is stabilized.

We introduced a combination of PFC with compliance control for fully actuated rigid body systems in [17], where the path is given as a regular parametrized curve. In [19], we presented first results of the stabilization of two-dimensional submanifolds (surface following control), which is closely related to [17] but not suitable for the combination with

Post-print version of the article: B. Bischof, T. Glück, M. Böck, and A. Kugi, "A path/surface following control approach to generate virtual fixtures", *IEEE Transactions on Robotics*, vol. 34, no. 6, pp. 1577–1592, 2018, ISSN: 1552-3098. DOI: 10.1109/TRO.2018.2861913
The content of this post-print version is identical to the published paper but without the publisher's final layout or copy editing.

compliance control. Open, closed, and intersecting surfaces represented by a regular parametrization of class $\mathcal{C}^3$ can be handled, which is in contrast to the approaches of [21], [22] that require the implicit representation of the surface. In [17] and [19], the manifold stabilization is only applied to the system output's position and the orientation is coupled to the resulting path or surface parameter. Also stability proofs of the dynamic closed-loop system with PFC and surface following control (SFC) are given.

Let us consider the dynamics of fully actuated rigid body systems of the form

$$\mathbf{D}(\mathbf{q})\ddot{\mathbf{q}} + \mathbf{n}(\mathbf{q}, \dot{\mathbf{q}}) = \boldsymbol{\tau}_d + \boldsymbol{\tau}_{\mathrm{ext}}, \tag{1}$$

with the generalized configuration coordinates $\mathbf{q} \in \mathbb{R}^m$, generalized actuator forces $\boldsymbol{\tau}_d \in \mathbb{R}^m$, external forces/torques $\boldsymbol{\tau}_{\mathrm{ext}} \in \mathbb{R}^m$, and the positive definite mass matrix $\mathbf{D}(\mathbf{q}) \in \mathbb{R}^{m \times m}$. The vector $\mathbf{n}(\mathbf{q}, \dot{\mathbf{q}})$ includes potential and friction forces as well as the centrifugal and Coriolis forces. The output function is given by

$$\mathbf{y} = \begin{bmatrix} \mathbf{y}_t \\ \mathbf{y}_r \end{bmatrix} = \begin{bmatrix} \mathbf{h}_t(\mathbf{q}) \\ \mathbf{h}_r(\mathbf{q}) \end{bmatrix} = \mathbf{h}(\mathbf{q}), \tag{2}$$

with the position $\mathbf{y}_t \in \mathbb{R}^3$, the orientation $\mathbf{y}_r \in \mathbb{R}^{m_r}$ in Cartesian coordinates, and $m = m_r + 3$. The Jacobian $\mathbf{J}(\mathbf{q}) = \partial\mathbf{h}/\partial\mathbf{q}$ is assumed to be nonsingular.

In robotics, the nonlinear system dynamics (1) are often neglected and the position and/or velocity of the joints are independently controlled using fast high bandwidth linear servo controllers. Feedforward of, e.g., the gravitational forces can be used to improve the performance of the subordinate velocity controllers. If the joint velocity controllers are assumed to be ideal, the system dynamics (1) simplifies to

$$\dot{\mathbf{q}} = \dot{\mathbf{q}}_{\mathrm{ref}} \ , \tag{3}$$

with the reference velocity input $\dot{\mathbf{q}}_{\mathrm{ref}}$.

In the following, we will introduce a combination of SFC with compliance control for the dynamic system (1) and (2), which features a (vector) relative degree of $\{2, 2, \dots, 2\}$, and we will call it dynamic SFC. The dynamic SFC is based on [19], but the coordinate transformation is enhanced such that a combination with compliance control is possible, which is essential for the generation of virtual fixtures. Additionally, we apply the SFC to the kinematic system (3), which drastically simplifies the control law compared to dynamic SFC. This simplified version will be called kinematic SFC. For the sake of readability and in view of the objective of this paper to systematically generate virtual fixtures, we will summarize the dynamic PFC of [17] and the kinematic PFC in Appendix A.

A. *Dynamic Surface Following Control (dynamic SFC)*

A smooth feedback law is designed that makes the robot's position $\mathbf{y}_t$ approach and move along a surface $\mathcal{S}_t$ with no a priori time parametrization, cf. Fig. 1.

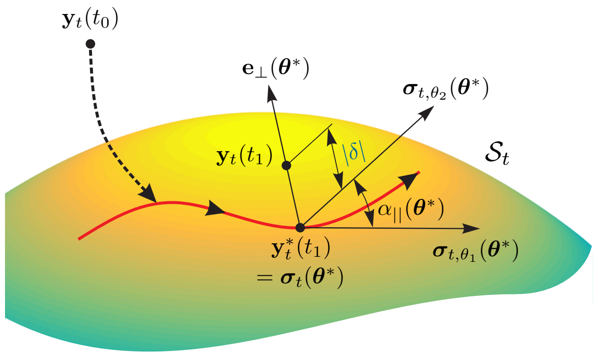

Fig. 1. Surface Following Control (SFC): Geometric description of the position part $\mathcal{S}_t$ and coordinate transformation.

1) Surface Assumptions: The surface $\mathcal{S}$ is given by a regular $\mathcal{C}^3$ parametrization $\boldsymbol{\sigma}^{\mathrm{T}}(\boldsymbol{\theta}) = \left[\boldsymbol{\sigma}_t^{\mathrm{T}}(\boldsymbol{\theta})\ \boldsymbol{\sigma}_r^{\mathrm{T}}(\boldsymbol{\theta})\right] : \mathcal{T}_s \mapsto \mathbb{R}^m$ with the parameter vector $\boldsymbol{\theta}^{\mathrm{T}} = \left[\theta_1\ \theta_2\right]$, which is element of a nonempty set $\mathcal{T}_s \subseteq \mathbb{R}^2$. The surface $\mathcal{S}$ can be separated into a position part $\mathcal{S}_t$ defined by $\boldsymbol{\sigma}_t(\boldsymbol{\theta})$ and an orientation part $\mathcal{S}_r$ defined by $\boldsymbol{\sigma}_r(\boldsymbol{\theta})$. The parametrization $\boldsymbol{\sigma}(\boldsymbol{\theta})$ of the surface $\mathcal{S}$ is regular, if $\boldsymbol{\sigma}_{t,\theta_1} \times \boldsymbol{\sigma}_{t,\theta_2} \neq \mathbf{0}$, $\forall\, \boldsymbol{\theta} \in \mathcal{T}_s$, where $\boldsymbol{\sigma}_{t,\theta_i} = \partial\boldsymbol{\sigma}_t/\partial\theta_i$ for $i = 1, 2$. Hence, at each point of the surface $\mathcal{S}_t$ there exist two linear independent tangent vectors $\boldsymbol{\sigma}_{t,\theta_i}$, $i = 1, 2$, with $\|\boldsymbol{\sigma}_{t,\theta_i}\| > 0$, and a normal unit vector $\mathbf{e}_\perp(\boldsymbol{\theta})$, which is the normalized cross product of the two tangent vectors, see Fig. 1.

2) Projection Operator: An orthogonal projection determines the closest point $\mathbf{y}_t^* = \boldsymbol{\sigma}_t(\boldsymbol{\theta}^*)$ on the surface $\mathcal{S}_t$ to $\mathbf{y}_t$. Therefore, the optimization problem

$$\boldsymbol{\theta}^* = \arg\min_{\boldsymbol{\theta} \in \mathcal{T}} f(\mathbf{y}_t, \boldsymbol{\theta}) \in \mathcal{T}_s \ , \tag{4}$$

with $f(\mathbf{y}_t, \boldsymbol{\theta}) = 1/2\|\mathbf{y}_t - \boldsymbol{\sigma}_t(\boldsymbol{\theta})\|_2^2$, is solved. We obtain the time-derivative of the optimal parameter vector $\boldsymbol{\theta}^*$ from the conditions of optimality as

$$\dot{\boldsymbol{\theta}}^* = \left(\frac{\partial^2 f}{\partial \boldsymbol{\theta}^2}\right)^{-1} (\mathbf{y}_t, \boldsymbol{\theta}^*) \begin{bmatrix} \boldsymbol{\sigma}_{t,\theta_1}^{\mathrm{T}}(\boldsymbol{\theta}^*) \\ \boldsymbol{\sigma}_{t,\theta_2}^{\mathrm{T}}(\boldsymbol{\theta}^*) \end{bmatrix} \dot{\mathbf{y}}_t \ . \tag{5}$$

Henceforth, the superscript $*$ always refers to a variable that is optimal with respect to the shortest distance to the surface $\mathcal{S}_t$. The conditions for the feasible neighborhood of the surface $\mathcal{S}_t$ in which (4) features a unique solution are given by, see [19],

$$\beta_1(\mathbf{y}_t) = E^* - \boldsymbol{\sigma}_{t,\theta_1\theta_1}^{\mathrm{T}}(\boldsymbol{\theta}^*)\left(\mathbf{y}_t - \boldsymbol{\sigma}_t(\boldsymbol{\theta}^*)\right) > 0 \ , \tag{6a}$$

$$\beta_2(\mathbf{y}_t) = \det\left(\frac{\partial^2 f}{\partial \boldsymbol{\theta}^2}(\mathbf{y}_t, \boldsymbol{\theta}^*)\right) > 0 \ , \tag{6b}$$

where $E^* = \boldsymbol{\sigma}_{t,\theta_1}^{\mathrm{T}}(\boldsymbol{\theta}^*)\boldsymbol{\sigma}_{t,\theta_1}(\boldsymbol{\theta}^*)$ and $\boldsymbol{\sigma}_{t,\theta_i\theta_j} = \partial^2\boldsymbol{\sigma}_t/\partial\theta_i\partial\theta_j$.

3) Coordinate Transformation: A coordinate transformation is defined which maps the generalized coordinates $\mathbf{q}$ into tangential coordinates, transversal coordinates, and rotational coordinates with respect to a surface $\mathcal{S}$. The angle between the tangent vectors $\boldsymbol{\sigma}_{t,\theta_1}$ and $\boldsymbol{\sigma}_{t,\theta_2}$ is given by $\alpha_{||}(\boldsymbol{\theta}) = \arccos\left(F/\sqrt{E\ G}\right)$, with $E = \boldsymbol{\sigma}_{t,\theta_1}^{\mathrm{T}}(\boldsymbol{\theta})\boldsymbol{\sigma}_{t,\theta_1}(\boldsymbol{\theta})$, $F = \boldsymbol{\sigma}_{t,\theta_1}^{\mathrm{T}}(\boldsymbol{\theta})\boldsymbol{\sigma}_{t,\theta_2}(\boldsymbol{\theta})$, and $G = \boldsymbol{\sigma}_{t,\theta_2}^{\mathrm{T}}(\boldsymbol{\theta})\boldsymbol{\sigma}_{t,\theta_2}(\boldsymbol{\theta})$, cf. Fig 1.

Post-print version of the article: B. Bischof, T. Glück, M. Böck, and A. Kugi, "A path/surface following control approach to generate virtual fixtures", *IEEE Transactions on Robotics*, vol. 34, no. 6, pp. 1577–1592, 2018, ISSN: 1552-3098. DOI: 10.1109/TRO.2018.2861913
The content of this post-print version is identical to the published paper but without the publisher's final layout or copy editing.

Note that due to the regularity of the surface $\mathcal{S}$, $\sin\left(\alpha_{||}(\boldsymbol{\theta})\right) \neq 0$ holds.

The tangential coordinates are defined by

$$\boldsymbol{\eta}_1 = \mathbf{g}(\mathbf{y}_t) = \int_{t_0}^{t} \boldsymbol{\Upsilon}^* \dot{\boldsymbol{\theta}}^* \mathrm{d}\tau \ , \tag{7}$$

with initial time t_0 and the nonsingular matrix

$$\boldsymbol{\Upsilon}^* = \begin{bmatrix} \|\boldsymbol{\sigma}_{t,\theta_1}(\boldsymbol{\theta}^*)\|_2 & \|\boldsymbol{\sigma}_{t,\theta_2}(\boldsymbol{\theta}^*)\|_2 \cos\left(\alpha_{||}(\boldsymbol{\theta}^*)\right) \\ 0 & \|\boldsymbol{\sigma}_{t,\theta_2}(\boldsymbol{\theta}^*)\|_2 \sin\left(\alpha_{||}(\boldsymbol{\theta}^*)\right) \end{bmatrix} ,$$

which ensures that the two components of $\boldsymbol{\eta}_1$ represent a physically interpretable length in orthogonal directions. This is in contrast to [19], where the feedback transformation is defined in a way that the tangential states $\boldsymbol{\eta}_1^{\mathrm{T}} = [\eta_{1,1}\ \eta_{1,2}]$ do not correspond to a physical length and are not orthogonal. Therefore, the approach proposed in [19] is not suitable for the combination with compliance control. Differentiation of (7) with respect to the time t yields

$$\begin{aligned} \dot{\boldsymbol{\eta}}_1 = \boldsymbol{\eta}_2 &= \boldsymbol{\Upsilon}^* \dot{\boldsymbol{\theta}}^* \\ &= \underbrace{\boldsymbol{\Upsilon}^* \left(\frac{\partial^2 f}{\partial \boldsymbol{\theta}^2}\right)^{-1} (\mathbf{y}_t, \boldsymbol{\theta}^*) \begin{bmatrix} \boldsymbol{\sigma}_{t,\theta_1}^{\mathrm{T}}(\boldsymbol{\theta}^*) \\ \boldsymbol{\sigma}_{t,\theta_2}^{\mathrm{T}}(\boldsymbol{\theta}^*) \end{bmatrix}}_{\nabla \mathbf{g} \in \mathbb{R}^{2\times 3}} \dot{\mathbf{y}}_t \ . \end{aligned} \tag{8}$$

The transversal coordinate ξ_1 is defined as the projection of $\mathbf{y}_t - \boldsymbol{\sigma}_t(\boldsymbol{\theta}^*)$ onto the normal unit vector $\mathbf{e}_\perp$, i.e.,

$$\xi_1 = \delta(\mathbf{y}_t) = \mathbf{e}_\perp^{\mathrm{T}}(\boldsymbol{\theta}^*)\left(\mathbf{y}_t - \boldsymbol{\sigma}_t(\boldsymbol{\theta}^*)\right) \ , \tag{9}$$

with time-derivative

$$\dot{\xi}_1 = \xi_2 = \underbrace{\mathbf{e}_\perp^{\mathrm{T}}(\boldsymbol{\theta}^*)}_{\nabla\delta^{\mathrm{T}}} \dot{\mathbf{y}}_t \ , \tag{10}$$

see [19]. The rotational coordinates are simply given by

$$\boldsymbol{\zeta}_1 = \mathbf{y}_r = \mathbf{h}_r(\mathbf{q}) \text{ and} \tag{11a}$$

$$\boldsymbol{\zeta}_2 = \dot{\boldsymbol{\zeta}}_1 = \frac{\partial \mathbf{h}_r(\mathbf{q})}{\partial \mathbf{q}} \dot{\mathbf{q}} = \mathbf{J}_r \dot{\mathbf{q}} \ . \tag{11b}$$

The virtual output $\hat{\mathbf{y}}_s^{\mathrm{T}} = \hat{\mathbf{h}}_s^{\mathrm{T}}(\mathbf{q}) = \left[\boldsymbol{\eta}_1^{\mathrm{T}}\ \xi_1\ \boldsymbol{\zeta}_1^{\mathrm{T}}\right]$ is introduced. Differentiation with respect to the time yields

$$\dot{\hat{\mathbf{y}}}_s = \mathbf{L}_s(\mathbf{q})\dot{\mathbf{y}} = \hat{\mathbf{J}}_s(\mathbf{q})\dot{\mathbf{q}} \ , \tag{12}$$

with the SFC Jacobian

$$\hat{\mathbf{J}}_s(\mathbf{q}) = \mathbf{L}_s(\mathbf{q})\mathbf{J}(\mathbf{q}) \tag{13}$$

and the matrices

$$\mathbf{L}_s(\mathbf{q}) = \begin{bmatrix} \mathbf{E}_s(\mathbf{q}) & \mathbf{0} \\ \mathbf{0} & \mathbf{I} \end{bmatrix} \quad \text{and} \quad \mathbf{E}_s(\mathbf{q}) = \begin{bmatrix} \nabla \mathbf{g} \\ \mathbf{e}_\perp^{\mathrm{T}} \end{bmatrix} ,$$

where $\mathbf{I}$ denotes the $m_r \times m_r$ identity matrix. Throughout this work, the subscript s in $\hat{\mathbf{y}}_s$, $\hat{\mathbf{h}}_s$, $\hat{\mathbf{J}}_s, \ldots$ refers to SFC, whereas the subscript p is used for the path following control approaches presented in Appendix A.

The coordinate transformation $\boldsymbol{\Phi} : \mathbb{R}^{2m} \to \mathbb{R}^{2m}$ maps the generalized coordinates $\mathbf{q}$ and $\dot{\mathbf{q}}$ to the tangential, transversal, and rotational coordinates $\hat{\mathbf{y}}_s$ and $\dot{\hat{\mathbf{y}}}_s$ and reads as

$$\begin{bmatrix} \hat{\mathbf{y}}_s \\ \dot{\hat{\mathbf{y}}}_s \end{bmatrix} = \begin{bmatrix} \mathbf{g} \circ \mathbf{h}_t(\mathbf{q}) \\ \delta \circ \mathbf{h}_t(\mathbf{q}) \\ \mathbf{h}_r(\mathbf{q}) \\ \hat{\mathbf{J}}_s(\mathbf{q})\dot{\mathbf{q}} \end{bmatrix} = \boldsymbol{\Phi}(\mathbf{q}, \dot{\mathbf{q}}) \ . \tag{14}$$

Lemma 1: The mapping $\boldsymbol{\Phi} : \mathcal{X} \mapsto \mathcal{Z}$ with $\mathcal{X} = \mathcal{Q} \times \mathcal{T}_{\mathbf{q}}\mathcal{Q}$, $\mathcal{Q} = \{\bar{\mathbf{q}} \in \mathbb{R}^m : \beta_i \circ \mathbf{h}_t(\bar{\mathbf{q}}) > 0,\ i = 1, 2\}$, and tangent space $\mathcal{T}_{\mathbf{q}}\mathcal{Q}$ is a $\mathcal{C}^1$-diffeomorphism, if $\mathbf{J}(\mathbf{q})$ is nonsingular.

Proof 1: Using the inverse function theorem, we have to show that

(i.) $\mathcal{X}$ and $\mathcal{Z}$ are open in $\mathbb{R}^{2m}$,
(ii.) $\boldsymbol{\Phi} \in \mathcal{C}^1(\mathcal{Q}, \mathcal{Z})$, and
(iii.) $\nabla\boldsymbol{\Phi} = \left[\partial\boldsymbol{\Phi}/\partial\mathbf{q}\quad \partial\boldsymbol{\Phi}/\partial\dot{\mathbf{q}}\right]$ is nonsingular for all $\left[\mathbf{q}^{\mathrm{T}}\quad \dot{\mathbf{q}}^{\mathrm{T}}\right]^{\mathrm{T}} \in \mathcal{X}$.

Since $\mathcal{Q}$ is an open subset of $\mathbb{R}^m$, $\mathcal{X}$ and $\mathcal{Z}$ are open in $\mathbb{R}^{2m}$. Moreover, the output $\mathbf{y} = \mathbf{h}(\mathbf{q})$ is assumed to be sufficiently smooth and $\boldsymbol{\sigma}(\boldsymbol{\theta}) \in \mathcal{C}^3(\mathcal{T}_s, \mathbb{R}^m)$, $\boldsymbol{\Phi} \in \mathcal{C}^1(\mathcal{X}, \mathcal{Z})$ holds. The Jacobian of $\boldsymbol{\Phi}$ reads as

$$\nabla\boldsymbol{\Phi} = \begin{bmatrix} \hat{\mathbf{J}}_s(\mathbf{q}) & \mathbf{0} \\ * & \hat{\mathbf{J}}_s(\mathbf{q}) \end{bmatrix} \ . \tag{15}$$

If $\mathbf{J}(\mathbf{q})$ is nonsingular and $\beta_i(\mathbf{y}_t) > 0,\ i = 1, 2$, then, $\mathbf{E}_s(\mathbf{q})$ and $\mathbf{L}_s(\mathbf{q})$ are nonsingular, and thus, $\hat{\mathbf{J}}_s$ and $\nabla\boldsymbol{\Phi}$ are nonsingular for all $\left[\mathbf{q}^{\mathrm{T}}\quad \dot{\mathbf{q}}^{\mathrm{T}}\right]^{\mathrm{T}} \in \mathcal{X}$.

4) Feedback Linearization: Differentiating (12) with respect to the time and inserting the system dynamics (1) yields

$$\ddot{\hat{\mathbf{y}}}_s = \dot{\hat{\mathbf{J}}}_s(\mathbf{q}, \dot{\mathbf{q}})\dot{\mathbf{q}} + \hat{\mathbf{J}}_s(\mathbf{q})\mathbf{D}^{-1}(\mathbf{q})\left(\boldsymbol{\tau}_d + \boldsymbol{\tau}_{ext} - \mathbf{n}(\mathbf{q}, \dot{\mathbf{q}})\right) \ . \tag{16}$$

Hence, application of the feedback transformation

$$\boldsymbol{\tau}_d = \mathbf{n}(\mathbf{q}, \dot{\mathbf{q}}) - \boldsymbol{\tau}_{ext} + \mathbf{D}(\mathbf{q})\hat{\mathbf{J}}_s^{-1}(\mathbf{q})\left(\mathbf{v}_s - \dot{\hat{\mathbf{J}}}_s(\mathbf{q}, \dot{\mathbf{q}})\dot{\mathbf{q}}\right) \tag{17}$$

to the system (1) with output function (2) results in a linear input-output relation from the new control input $\mathbf{v}_s^{\mathrm{T}} = \left[\mathbf{v}_{s,t}^{\mathrm{T}}\quad \mathbf{v}_{s,r}^{\mathrm{T}}\right]$, where $\mathbf{v}_{s,t}^{\mathrm{T}} = \left[v_{||,1}\quad v_{||,2}\quad v_\perp\right]$, to the virtual output $\hat{\mathbf{y}}_s$ in the form of m integrator chains of length two

$$\ddot{\hat{\mathbf{y}}}_s = \mathbf{v}_s \ . \tag{18}$$

Any controller that stabilizes the linearized system (18) can be used to compute the new control input $\mathbf{v}_s$. In the following, a position controller and a compliance controller for the dynamic SFC to compute $\mathbf{v}_s$ will be presented.

5) Position Control: The position control law

$$\mathbf{v}_s = \begin{bmatrix} \mathbf{v}_{s,t} \\ \mathbf{v}_{s,r} \end{bmatrix} = \begin{bmatrix} \ddot{\boldsymbol{\eta}}_1^p - a_{\eta,2}\dot{\mathbf{e}}_\eta^p - a_{\eta,1}\mathbf{e}_\eta^p \\ \ddot{\xi}_1^p - a_{\xi,2}\dot{e}_{\xi_1}^p - a_{\xi,1}e_{\xi_1}^p \\ \ddot{\mathbf{y}}_r^p - a_{r,2}\dot{\mathbf{e}}_r^p - a_{r,1}\mathbf{e}_r^p \end{bmatrix} , \tag{19}$$

where $\mathbf{e}_\eta^p = \boldsymbol{\eta}_1 - \boldsymbol{\eta}_1^p$, $e_{\xi_1}^p = \xi_1 - \xi_1^p$, and $\mathbf{e}_r^p = \mathbf{y}_r - \mathbf{y}_r^p$, yields the exponentially stable error dynamics

$$\begin{bmatrix} \ddot{\mathbf{e}}_\eta^p + a_{\eta,2}\dot{\mathbf{e}}_\eta^p + a_{\eta,1}\mathbf{e}_\eta^p \\ \ddot{e}_{\xi_1}^p + a_{\xi,2}\dot{e}_{\xi_1}^p + a_{\xi,1}e_{\xi_1}^p \\ \ddot{\mathbf{e}}_r^p + a_{r,2}\dot{\mathbf{e}}_r^p + a_{r,1}\mathbf{e}_r^p \end{bmatrix} = \mathbf{0} \ , \tag{20}$$

for $a_{i,j} > 0$ with $i \in \{\eta, \xi, r\}$ and $j = 1, 2$. The $\mathcal{C}^2$ reference position on the surface is denoted by $\boldsymbol{\eta}_1^p$ and the $\mathcal{C}^2$ reference for the transversal state by ξ_1^p, where the superscript p designates references for position controllers throughout this work. The reference for the orientation is given by $\mathbf{y}_r^p = \boldsymbol{\sigma}_r(\boldsymbol{\theta}^*)$. Note that integral parts can also be added to the control law (19) to eliminate the control errors in stationary conditions.

Post-print version of the article: B. Bischof, T. Glück, M. Böck, and A. Kugi, "A path/surface following control approach to generate virtual fixtures", *IEEE Transactions on Robotics*, vol. 34, no. 6, pp. 1577–1592, 2018, ISSN: 1552-3098. DOI: 10.1109/TRO.2018.2861913
The content of this post-print version is identical to the published paper but without the publisher's final layout or copy editing.

6) Compliance Control: A compliance controller enables a reference dynamics (impedance) between the measured external forces and the position. Here, an approach closely related to [23] is utilized, where the trajectory of the exponentially stable reference impedance model is tracked by the position controller (19). With the SFC, the reference impedance of the motion along and orthogonal to the surface as well as the reference impedance of the orientation can be separately defined as

$$\begin{bmatrix}\boldsymbol{\tau}_{||}\\ \tau_{\perp}\\ \boldsymbol{\tau}_r\end{bmatrix} = \begin{bmatrix} m_{||}^d\ddot{\mathbf{e}}_\eta^d + d_{||}^d\dot{\mathbf{e}}_\eta^d + k_{||}^d\mathbf{e}_\eta^d\\ m_\perp^d\ddot{e}_\xi^d + d_\perp^d\dot{e}_\xi^d + k_\perp^d e_\xi^d\\ m_r^d\ddot{\mathbf{e}}_r^d + d_r^d\dot{\mathbf{e}}_r^d + k_r^d\mathbf{e}_r^d\end{bmatrix} , \tag{21}$$

where $\mathbf{e}_\eta^d = \boldsymbol{\eta}_1 - \boldsymbol{\eta}_1^d$ and $e_\xi^d = \xi_1 - \xi_1^d$ denote the errors between the coordinates $\boldsymbol{\eta}_1$, ξ_1 and the $\mathcal{C}^2$ references $\boldsymbol{\eta}_1^d$, ξ_1^d and $\mathbf{e}_r^d = \mathbf{y}_r - \boldsymbol{\sigma}_r(\theta^*)$. Moreover, m_i^d, d_i^d, and k_i^d for $i \in \{||, \perp, r\}$ are positive design parameters. The external (projected) generalized forces are given by

$$\begin{bmatrix}\boldsymbol{\tau}_{||}\\ \tau_{\perp}\\ \boldsymbol{\tau}_r\end{bmatrix} = \hat{\mathbf{J}}_s^{-\mathrm{T}}\boldsymbol{\tau}_{\text{ext}} . \tag{22}$$

The controller (19) is used as inner position control loop and assuming perfect tracking, the actual tangential and transversal coordinates $\boldsymbol{\eta}_1$ and ξ_1 as well as the orientation $\mathbf{y}_r$ in (21) can be replaced by the position controller references $\boldsymbol{\eta}_1^p$, ξ_1^p, and $\mathbf{y}_r^p$. The impedance control law then follows as

$$\ddot{\boldsymbol{\eta}}_1^p = \ddot{\boldsymbol{\eta}}_1^d + \frac{\boldsymbol{\tau}_{||}}{m_{||}^d} - \frac{d_{||}^d}{m_{||}^d}\dot{\mathbf{e}}_\eta^{pd} - \frac{k_{||}^d}{m_{||}^d}\mathbf{e}_\eta^{pd} ,$$
$$\dot{\boldsymbol{\eta}}_1^p = \int_0^t \ddot{\boldsymbol{\eta}}_1^p \mathrm{d}\tau, \quad \boldsymbol{\eta}_1^p = \int_0^t \dot{\boldsymbol{\eta}}_1^p\mathrm{d}\tau , \tag{23a}$$

$$\ddot{\xi}_1^p = \ddot{\xi}_1^d + \frac{\tau_\perp}{m_\perp^d} - \frac{d_\perp^d}{m_\perp^d}\dot{e}_{\xi_1}^{pd} - \frac{k_\perp^d}{m_\perp^d}e_{\xi_1}^{pd} ,$$
$$\dot{\xi}_1^p = \int_0^t \ddot{\xi}_1^p\mathrm{d}\tau, \quad \xi_1^p = \int_0^t \dot{\xi}_1^p\mathrm{d}\tau , \tag{23b}$$

$$\ddot{\mathbf{y}}_r^p = \ddot{\boldsymbol{\sigma}}_r(\theta^*) + \frac{\boldsymbol{\tau}_r}{m_r^d} - \frac{d_r^d}{m_r^d}\dot{\mathbf{e}}_r^{pd} - \frac{k_r^d}{m_r^d}\mathbf{e}_r^{pd} ,$$
$$\dot{\mathbf{y}}_r^p = \int_0^t \ddot{\mathbf{y}}_r^p\mathrm{d}\tau, \quad \mathbf{y}_r^p = \int_0^t \dot{\mathbf{y}}_r^p\mathrm{d}\tau , \tag{23c}$$

with the errors $\mathbf{e}_\eta^{pd} = \boldsymbol{\eta}_1^p - \boldsymbol{\eta}_1^d$, $e_{\xi_1}^{pd} = \xi_1^p - \xi_1^d$, and $\mathbf{e}_r^{pd} = \mathbf{y}_r^p - \boldsymbol{\sigma}_r(\theta^*)$. Hence, in the combination of SFC with compliance control, the (external) references in tangential and orthogonal direction to the surface $\mathcal{S}$ are denoted by the superscript d and the references for the inner position control loop are denoted by the superscript p.

In the three-dimensional space, the orientation $\mathbf{y}_r \in \mathbb{R}^3$ is often represented by Euler angles $\boldsymbol{\phi}_e^{\mathrm{T}} = \begin{bmatrix}\varphi_e \ \vartheta_e \ \psi_e\end{bmatrix}$. They suffer from representation singularities and the impedance depends on the orientation of the compliant frame with respect to the inertial frame when using the position control law (19) to compute $\mathbf{v}_{s,r}$ together with the compliance control (23c), cf. [24]. To avoid these disadvantages, the approach of [24] is adapted for SFC. Using the geometric Jacobian $\mathbf{J}_g$ according to (48), see Appendix B, instead of $\mathbf{J}$ in (13) to compute $\hat{\mathbf{J}}_s$ for the SFC feedback transformation (17) yields the linear systems $\ddot{\mathbf{y}}_s^{\mathrm{T}} = \begin{bmatrix}\ddot{\boldsymbol{\eta}}_1^{\mathrm{T}} \ \ddot{\xi}_1 \ \dot{\boldsymbol{\omega}}_e^{\mathrm{T}}\end{bmatrix} = \begin{bmatrix}\mathbf{v}_{s,t}^{\mathrm{T}} \ \mathbf{v}_{s,o}^{\mathrm{T}}\end{bmatrix}$, where $\boldsymbol{\omega}_e$ denotes the angular velocity of the end-effector expressed in the inertial frame. We define the orientation between the compliant frame p and the desired frame d as

$$\mathbf{R}_p^d = \mathbf{R}_d^{\mathrm{T}}\mathbf{R}_p , \tag{24}$$

where $\mathbf{R}_d$ is the rotation matrix of the reference Euler angles $\boldsymbol{\phi}_d = \boldsymbol{\sigma}_r(\theta^*)$ and $\mathbf{R}_p$ is the rotation matrix of the compliant frame and define the impedance as

$$m_r^d\ddot{\boldsymbol{\phi}}_{pd} + d_r^d\dot{\boldsymbol{\phi}}_{pd} + k_r^d\boldsymbol{\phi}_{pd} = \boldsymbol{\mu}^d \tag{25}$$

where $\boldsymbol{\phi}_{pd}^{\mathrm{T}} = \begin{bmatrix}\varphi_{pd} \ \vartheta_{pd} \ \psi_{pd}\end{bmatrix}$ are the ZYX Euler angles of $\mathbf{R}_p^d$. In (25), $(\boldsymbol{\mu}^d)^{\mathrm{T}} = [\mu_\varphi^d \ \ \mu_\vartheta^d \ \ \mu_\psi^d]$ is the transformed measured torque vector $\boldsymbol{\mu}^d = \mathbf{T}^{\mathrm{T}}(\boldsymbol{\phi}_{pd})[\mathbf{0} \quad \mathbf{R}_d^{\mathrm{T}}]\mathbf{J}_g^{-\mathrm{T}}\boldsymbol{\tau}_{ext}$, with the transformation $\mathbf{T}(\cdot)$ given by (47) and the geometric Jacobian $\mathbf{J}_g$ of (48), see Appendix B. Note that representation singularities do not appear in (25) for $|\vartheta_{pd}| < \pi/2$.

The control law

$$\mathbf{v}_{s,o} = \dot{\boldsymbol{\omega}}_d + \dot{\mathbf{B}}_d(\boldsymbol{\phi}_{ed})\dot{\boldsymbol{\phi}}_{ed} + \mathbf{B}_d(\boldsymbol{\phi}_{ed})\left(\ddot{\boldsymbol{\phi}}_{pd} + a_{o,2}\left(\dot{\boldsymbol{\phi}}_{pd} - \dot{\boldsymbol{\phi}}_{ed}\right) + a_{o,1}\left(\boldsymbol{\phi}_{pd} - \boldsymbol{\phi}_{ed}\right)\right) \tag{26}$$

with $\mathbf{B}_d(\boldsymbol{\phi}_{ed}) = \mathbf{R}_d\mathbf{T}(\boldsymbol{\phi}_{ed})$ and $\boldsymbol{\phi}_{ed}$ as the ZYX Euler angles of $\mathbf{R}_e^d$ leads to the exponentially stable error dynamics

$$\ddot{\boldsymbol{\phi}}_{ed} - \ddot{\boldsymbol{\phi}}_{pd} + a_{o,2}\left(\dot{\boldsymbol{\phi}}_{ed} - \dot{\boldsymbol{\phi}}_{pd}\right) + a_{o,1}\left(\boldsymbol{\phi}_{ed} - \boldsymbol{\phi}_{pd}\right) = \mathbf{0} , \tag{27}$$

for $a_{o,1} > 0$ and $a_{o,2} > 0$, cf. [24]. Hence, the orientation of the end-effector $\mathbf{R}_e$ converges to the desired compliant orientation $\mathbf{R}_p$.

B. Kinematic Surface Following Control (kinematic SFC)

The SFC introduced in the last section can be drastically simplified when ideal subordinate velocity controllers are presumed and thus relation (3) is satisfied. The simplified approach for the system (3) with output function (2) is referred to as kinematic SFC. In contrast to the dynamic SFC, the surface parametrization $\boldsymbol{\sigma}(\boldsymbol{\theta})$ has only to be $\mathcal{C}^2$ because the (vector) relative degree of the system reduces to $\{1, 1, \ldots, 1\}$.

The coordinate transformation $\boldsymbol{\Phi}_k : \mathbb{R}^m \to \mathbb{R}^m$ maps the generalized coordinates $\mathbf{q}$ to the tangential, transversal, and rotational coordinates $\hat{\mathbf{y}}_s$ and reads as

$$\hat{\mathbf{y}}_s = \begin{bmatrix}\mathbf{g}\circ\mathbf{h}_t(\mathbf{q})\\ \delta\circ\mathbf{h}_t(\mathbf{q})\\ \mathbf{h}_r(\mathbf{q})\end{bmatrix} = \boldsymbol{\Phi}_k(\mathbf{q}) , \tag{28}$$

with $\mathbf{g}$ and δ from (7) and (9), respectively. The same considerations as in Proof 1 lead to the finding that $\boldsymbol{\Phi}_k$ is a $\mathcal{C}^1$-diffeomorphism in the feasible neighborhood of the surface $\mathcal{S}$.

Because of (12), application of the feedback transformation

$$\dot{\mathbf{q}}_{ref} = \hat{\mathbf{J}}_s^{-1}\mathbf{v}_{s,k} \tag{29}$$

Post-print version of the article: B. Bischof, T. Glück, M. Böck, and A. Kugi, "A path/surface following control approach to generate virtual fixtures", *IEEE Transactions on Robotics*, vol. 34, no. 6, pp. 1577–1592, 2018, ISSN: 1552-3098. DOI: 10.1109/TRO.2018.2861913
The content of this post-print version is identical to the published paper but without the publisher's final layout or copy editing.

to the system (3), with new control input $\mathbf{v}_{s,k}^{\mathrm{T}} = \left[\mathbf{v}_{s,k,t}^{\mathrm{T}}\ \mathbf{v}_{s,k,r}^{\mathrm{T}}\right]$, where $\mathbf{v}_{s,k,t}^{\mathrm{T}} = \left[v_{k,||,1}\ v_{k,||,2}\ v_{k,\perp}\right]$, results in a linear input-output relation from the new control input $\mathbf{v}_{s,k}$ to the virtual SFC output $\hat{\mathbf{y}}_s$ in the form of m decoupled integrators

$$\dot{\hat{\mathbf{y}}}_s = \mathbf{v}_{s,k} \ . \tag{30}$$

Unlike the SFC feedback law for the dynamic model, see (17), the computational demanding time-derivative of the Jacobian $\dot{\hat{\mathbf{J}}}_s$ does not appear in the kinematic SFC control law (29).

The position control law

$$\mathbf{v}_{s,k} = \begin{bmatrix}\mathbf{v}_{s,k,t}\\ \mathbf{v}_{s,k,r}\end{bmatrix} = \begin{bmatrix}\dot{\boldsymbol{\eta}}_1^p - a_\eta \mathbf{e}_\eta^p\\ \dot{\xi}_1^p - a_\xi e_\xi^p\\ \dot{\mathbf{y}}_r^p - a_r \mathbf{e}_r^p\end{bmatrix} \ , \tag{31}$$

where $\mathbf{e}_\eta^p = \boldsymbol{\eta}_1 - \boldsymbol{\eta}_1^p$, $e_\xi^p = \xi_1 - \xi_1^p$, and $\mathbf{e}_r^p = \mathbf{y}_r - \mathbf{y}_r^p$, yields an exponentially stable error dynamics, if $a_i > 0$ with $i \in \{\eta, \xi, r\}$. The impedance control law to compute the references $\boldsymbol{\eta}_1^p$, ξ_1^p, and $\mathbf{y}_r^p$ is identical to the dynamic SFC given in (23).

As for the dynamic SFC, the computation of $\mathbf{v}_{s,k,r}$ with (31) and (23c) suffers from representation singularities in the case of $\mathbf{y}_r \in \mathbb{R}^3$. To avoid these disadvantages, the approach of [24] is adapted for the kinematic SFC.

Using the geometric Jacobian in (13), i.e., $\mathbf{J} = \mathbf{J}_g$, for the SFC feedback transformation (29) yields the linear system $\dot{\hat{\mathbf{y}}}_s^{\mathrm{T}} = [\dot{\boldsymbol{\eta}}_1^{\mathrm{T}}\ \dot{\xi}_1\ \boldsymbol{\omega}_e^{\mathrm{T}}] = [\mathbf{v}_{s,k,t}^{\mathrm{T}}\ \mathbf{v}_{s,k,o}^{\mathrm{T}}]$. The control law

$$\mathbf{v}_{s,k,o} = \boldsymbol{\omega}_p - \mathbf{B}_p(\boldsymbol{\phi}_{ep}) a_r \boldsymbol{\phi}_{ep} \ , \tag{32}$$

with $\mathbf{B}_p(\boldsymbol{\phi}_{ep}) = \mathbf{R}_p \mathbf{T}(\boldsymbol{\phi}_{ep})$, where $\mathbf{R}_p$ is computed from (24), and $\boldsymbol{\phi}_{ep}$ as the ZYX Euler angles of $\mathbf{R}_e^p = \mathbf{R}_p^{\mathrm{T}} \mathbf{R}_e$, leads to the exponentially stable error dynamics

$$\dot{\boldsymbol{\phi}}_{ep} + a_r \boldsymbol{\phi}_{ep} = \mathbf{0} \ , \tag{33}$$

with $a_r > 0$. For this derivation, the relations $\boldsymbol{\omega}_{pd}^d = \mathbf{T}(\boldsymbol{\phi}_{pd})\dot{\boldsymbol{\phi}}_{pd}$, $\boldsymbol{\omega}_p = \boldsymbol{\omega}_d + \mathbf{R}_d \boldsymbol{\omega}_{pd}^d$, $\boldsymbol{\omega}_d = \mathbf{T}\big(\boldsymbol{\sigma}_r(\theta^*)\big)\boldsymbol{\sigma}_r'(\theta^*)\dot{\theta}^*$, and $\boldsymbol{\omega}_{ep} = \boldsymbol{\omega}_e - \boldsymbol{\omega}_p = \mathbf{R}_p \boldsymbol{\omega}_{ep}^p = \mathbf{B}_p(\boldsymbol{\phi}_{ep})\dot{\boldsymbol{\phi}}_{ep}$ are used.

III. Generating Virtual Fixtures using PFC and SFC

The PFC and SFC approaches presented in Section II and Appendix A decouple and exactly linearize the dynamics in tangential and orthogonal direction to a path or surface. Thereby, PFC and SFC is only applied to the position parametrization of a path or a surface, γ_t and $\mathcal{S}_t$, respectively. The reference orientation is coupled to the optimal path parameter θ^* (or optimal surface parameter vector $\boldsymbol{\theta}^*$) and given by the trajectory $\mathbf{y}_r^p(t) = \boldsymbol{\sigma}_r(\theta^*(t))$. Hence, the behavior of the system along a path or surface and away from it can be defined independently and, furthermore, in a physically interpretable manner, which allows to realize a large number of possible virtual fixtures. In contrast to other virtual fixture methods, a systematic proof of the closed-loop stability including the dynamics of the manipulator can be given. A compliant behavior of the manipulator is achieved by measuring the external force introduced by an operator $\mathbf{f}_{op} = \mathbf{J}_g^{-\mathrm{T}} \boldsymbol{\tau}_{\mathrm{ext}}$ and using the impedance control laws (23) or (42) presented in the Section II and Appendix A, respectively. Note that for systems with very low (or compensated) friction, compliance can also be achieved without a force sensor by dynamic PFC/SFC and the position control (19) or (41) with small gains. For such systems, the operator's input force $\mathbf{f}_{op}$ can be estimated from the drive forces/torques $\boldsymbol{\tau}_d$.

The survey papers [2] and [7] distinguish between several properties and classifications of virtual fixtures. Numerous methods to define the geometry of the virtual fixtures can be found in literature including point clouds and mesh grids. The paths for PFC and the surfaces for SFC can be defined by splines allowing to approximate the geometry of the constraints and, additionally, leading to a continuous control output. Three classifications of virtual fixtures that can be generated with PFC and SFC are discussed in the following and are experimentally validated in Section V.

A. Guidance and Forbidden Region Virtual Fixtures

Virtual fixtures can either guide an operator to and along a submanifold of the workspace (guidance virtual fixture) or prevent the operator from entering specific areas of the workspace (forbidden region virtual fixture). Most of the existing methods to generate virtual fixtures enable only one of the two possibilities.

PFC and SFC ensure that the manipulator converges to and then remains on a path or surface. Compliance control in tangential direction with low stiffness and damping enables the operator to easily move the manipulator along the path or surface. Hence, guidance virtual fixtures can be implemented using kinematic or dynamic PFC/SFC by simply adjusting the parameters in the position controllers and the impedance control laws (23) and (42), respectively.

In the case of forbidden region virtual fixtures, the operator is able to move the manipulator's end-effector freely inside the feasible region of the restricted workspace without any manifold stabilization. Various control concepts like Cartesian impedance control exist to generate such an unconstrained motion, e.g., [25], [26], [27], [23], [28]. The limits of the restricted workspace are defined by M parametrized surfaces $\mathcal{S}_{t,i}$, $i = 1, \ldots, M$, and inside its feasible region, the shortest distance to each surface has to be computed. This can be achieved by solving a global optimization problem to obtain each optimal surface parameter vector $\boldsymbol{\theta}_i^*$, which is in general computationally quite intensive. SFC with the corresponding surface $\mathcal{S}_{t,i}$ gets activated to prevent from entering the forbidden region, when the manipulator's end-effector contacts $\mathcal{S}_{t,i}$ and the input force of the operator $\mathbf{f}_{op}$ points into the forbidden region, implying that $\|\mathbf{y}_t - \boldsymbol{\sigma}_{t,i}(\boldsymbol{\theta}_i^*)\| < d_{fr}$ as well as $s_{fr,i}\mathbf{e}_{i,\perp}^{\mathrm{T}}(\boldsymbol{\theta}_i^*)[\mathbf{I}\ \mathbf{0}]\mathbf{f}_{op} < 0$ holds, where $\boldsymbol{\sigma}_{t,i}$ is the position parametrization of the surface $\mathcal{S}_{t,i}$, $d_{fr} > 0$ is the distance threshold, $\mathbf{I}$ is the 3×3 identity matrix, and $s_{fr,i} = 1$ when the normal vector $\mathbf{e}_{i,\perp}$ onto the surface $\mathcal{S}_{t,i}$ points into the feasible area and $s_{fr,i} = -1$ when $\mathbf{e}_{i,\perp}$ points into the forbidden region. The motion is then restricted by SFC to a tangential direction of the surface $\mathcal{S}_{t,i}$ as long as the operator's input force $\mathbf{f}_{op}$ points into the forbidden region. Unconstrained motion is activated again once the input force of the operator points into the feasible area, i.e., $s_{fr,i}\mathbf{e}_{i,\perp}^{\mathrm{T}}(\boldsymbol{\theta}_i^*)[\mathbf{I}\ \mathbf{0}]\mathbf{f}_{op} > f_{fr}$

Post-print version of the article: B. Bischof, T. Glück, M. Böck, and A. Kugi, "A path/surface following control approach to generate virtual fixtures", *IEEE Transactions on Robotics*, vol. 34, no. 6, pp. 1577–1592, 2018, ISSN: 1552-3098. DOI: 10.1109/TRO.2018.2861913
The content of this post-print version is identical to the published paper but without the publisher's final layout or copy editing.

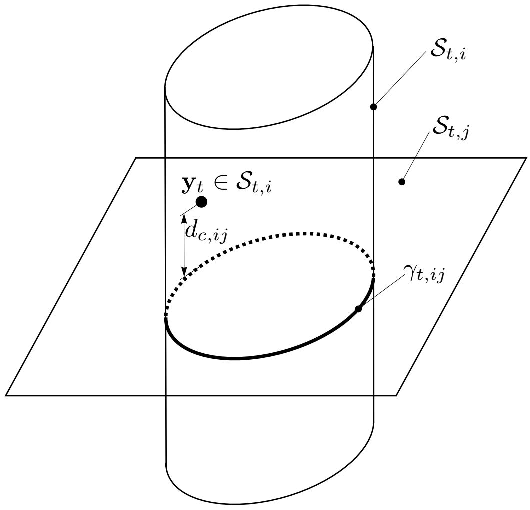

Fig. 2. Intersection of two surfaces.

holds, where $f_{fr} > 0$ is a small force threshold that prevents from chattering between the control laws.

Assume that the two surfaces $\mathcal{S}_{t,i}$ and $\mathcal{S}_{t,j}$ intersect in the curve $\gamma_{t,ij}$ as depicted in Fig. 2. Then, during active SFC with surface $\mathcal{S}_{t,i}$, $\mathbf{y}_t \in \mathcal{S}_{t,i}$ holds, and the shortest distance $d_{c,ij}$ to the intersection curve $\gamma_{t,ij}$ has to be computed. Once the manipulator's end-effector contacts the intersection curve $\gamma_{t,ij}$, thus also the surface $\mathcal{S}_{t,j}$, and the operator's input force $\mathbf{f}_{op}$ points into the forbidden region of the surface $\mathcal{S}_{t,j}$, i.e., $d_{c,ij} = \|\mathbf{y}_t - \boldsymbol{\sigma}_{t,j}(\boldsymbol{\theta}_j^*)\| < d_{fr}$ as well as $s_{fr,j}\mathbf{e}_{j,\perp}^{\mathrm{T}}(\boldsymbol{\theta}_j^*)[\mathbf{I}\ \mathbf{0}]\mathbf{f}_{op} < 0$ holds, PFC along the intersection curve $\gamma_{t,ij}$ gets activated. With active PFC, the optimal parameter vectors $\boldsymbol{\theta}_i^*$ and $\boldsymbol{\theta}_j^*$ of the two intersecting surfaces have to be computed to be able to switch back to SFC. The transition back to SFC with surface $\mathcal{S}_{t,i}$ takes place when $s_{fr,j}\mathbf{e}_{j,\perp}^{\mathrm{T}}(\boldsymbol{\theta}_j^*)[\mathbf{I}\ \mathbf{0}]\mathbf{f}_{op} > f_{fr}$ holds and the transition to SFC with surface $\mathcal{S}_{t,j}$ takes place when $s_{fr,i}\mathbf{e}_{i,\perp}^{\mathrm{T}}(\boldsymbol{\theta}_i^*)[\mathbf{I}\ \mathbf{0}]\mathbf{f}_{op} > f_{fr}$ holds. The resulting state machine to generate forbidden region virtual fixtures with SFC and PFC is depicted in Fig. 3. Note that in the special case of three intersecting surfaces in one point, set-point stabilization has to be added as control state with similar transitions to PFC as described above.

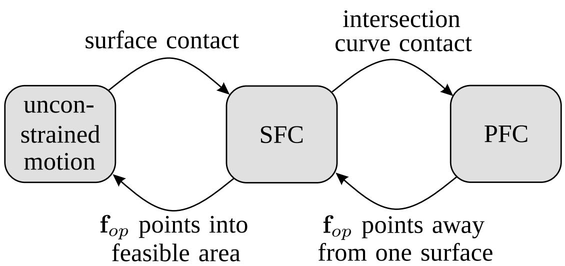

Fig. 3. Forbidden region virtual fixtures state machine.

It is worth noting that we do not provide a stability proof for the overall switched system including the state machine of Fig. 3. While this is not a big issue for static forbidden region virtual fixtures, it has to be investigated in more detail for the dynamic case.

B. Hard and Soft Constraints

The behavior away from the virtual fixture defines the level of guidance. Hard constraints do not allow any motion off the virtual fixture (negligible deviations always occur in practice due to limited control gains), while soft constraints give some compliance to allow the operator little freedom to deviate from the fixture.

Hard constraints can be implemented with kinematic or dynamic PFC/SFC by using the position controller (19), (31), (41), or (45) for the orthogonal directions with high gains.

Using the combination of compliance control with PFC or SFC enables to realize soft constraints. The stiffness away from the constraint can be adjusted with $k_\perp^d$. The impedance control laws (23) and (42) remain stable for a variable stiffness $k_\perp^d = k_\perp^d(\xi_i) > 0$, with $i = 1, 3$. Hence, also nonlinear virtual springs can be implemented. Note that for manipulators with very low (or compensated) friction, soft constraints can also be generated by using dynamic PFC/SFC together with the position controller (19) or (41) for the orthogonal directions with small gains.

C. Static and Dynamic Virtual Fixtures

Normally, the virtual fixtures do not change over time and are static. However, in some applications the constraints have to be changed dynamically to adapt to a changing environment, e.g., in robot-assisted heart surgery [29].

Such dynamic virtual fixtures can also be implemented with PFC or SFC. Thereby, the path γ_t or surface $\mathcal{S}_t$ remains constant, but the reference path or surface deviation is adapted corresponding to the dynamic virtual fixture. For PFC, the desired path deviation $\Delta\boldsymbol{\sigma}_t(t) \in \mathcal{C}^2$ at $\boldsymbol{\sigma}_t(\theta^*)$ is projected onto the normal vectors $\mathbf{e}_\perp$ and $\mathbf{e}_\pitchfork$ leading to the transversal references

$$\xi_1^i = \mathbf{e}_\perp^{\mathrm{T}} \Delta\boldsymbol{\sigma}_t \quad \text{and} \quad \xi_3^i = \mathbf{e}_\pitchfork^{\mathrm{T}} \Delta\boldsymbol{\sigma}_t \ , \tag{34}$$

where $i = p$ for hard constraints and $i = d$ for soft constraints. For SFC, there is only one transversal direction onto the surface $\mathcal{S}_t$ and, hence, the transversal reference is given by

$$\xi_1^i = \Delta\sigma_t \ , \tag{35}$$

with $i = p$ for hard constraints, $i = d$ for soft constraints, and the scalar desired surface deviation $\Delta\sigma_t(t) \in \mathcal{C}^2$.

A desired path deviation of class $\mathcal{C}^2$ implies a continuous output $\boldsymbol{\tau}_d$ or $\dot{\mathbf{q}}_{\mathrm{ref}}$, respectively, of the PFC/SFC feedback transformation. Note that the maximum deviation from a path or surface is limited by the feasible neighborhood, see [17] and [19].

Post-print version of the article: B. Bischof, T. Glück, M. Böck, and A. Kugi, "A path/surface following control approach to generate virtual fixtures", *IEEE Transactions on Robotics*, vol. 34, no. 6, pp. 1577–1592, 2018, ISSN: 1552-3098. DOI: 10.1109/TRO.2018.2861913
The content of this post-print version is identical to the published paper but without the publisher's final layout or copy editing.

TABLE I
GUIDANCE VIRTUAL FIXTURES FOR MANIPULATORS WITH FORCE SENSOR.

guidance virtual fixture type			control laws	
stat./dyn. manifold	guidance level	manifold type	dynamic PFC/SFC	kinematic PFC/SFC
static	hard	path	(39),(41),(42a)	(43),(45),(42a)
		surface	(17),(19),(23a)	(29),(31),(23a)
	soft	path	(39),(41),(42)	(43),(45),(42)
		surface	(17),(19),(23)	(29),(31),(23)
dynamic	hard	path	(39),(41) (42a),(34)	(43),(45) (42a),(34)
		surface	(17),(19) (23a),(35)	(29),(31) (23a),(35)
	soft	path	(39),(41) (42),(34)	(43),(45) (42),(34)
		surface	(17),(19) (23),(35)	(29),(31) (23),(35)

D. Summary

A large number of virtual fixtures can be generated with PFC and SFC by combining the methods described in this section. Tab. I lists the types of guidance virtual fixtures that can be generated with either dynamic or kinematic PFC/SFC for a manipulator equipped with a sensor to measure the forces introduced by an operator as well as the required control laws. If the manipulator has very low (or compensated) friction, it is highly back-drive-able and virtual fixtures can be generated using PFC/SFC without a force sensor. In this case, kinematic PFC/SFC cannot be used due to the high gains of the velocity controllers. The types of guidance virtual fixtures that can be generated with dynamic PFC/SFC for a highly back-drive-able manipulator without force sensor are listed in Tab. II.

TABLE II
GUIDANCE VIRTUAL FIXTURES FOR BACK-DRIVE-ABLE MANIPULATORS.

guidance virtual fixture type			control laws
static/dynamic manifold	guidance level	manifold type	dynamic PFC/SFC
static	hard	path	(39),(41)
		surface	(17),(19)
	soft	path	(39),(41)
		surface	(17),(19)
dynamic	hard	path	(39),(41),(34)
		surface	(17),(19),(35)
	soft	path	(39),(41),(34)
		surface	(17),(19),(35)

Compared to guidance virtual fixtures, the generation of forbidden region virtual fixtures with PFC/SFC requires more implementation and computational effort due to the switching between the control laws. With the described method, only static forbidden region virtual fixtures with hard constraints can be generated, where the same control laws as listed in Tab. I or Tab. II for a static manifold and hard guidance level are used. Dynamic virtual fixtures or soft constraints require different switching strategies, which are subject to further research.

IV. EXPERIMENTAL VALIDATION OF THE DYNAMIC SFC

The combination of the dynamic SFC with compliance control introduced in Section II is experimentally validated

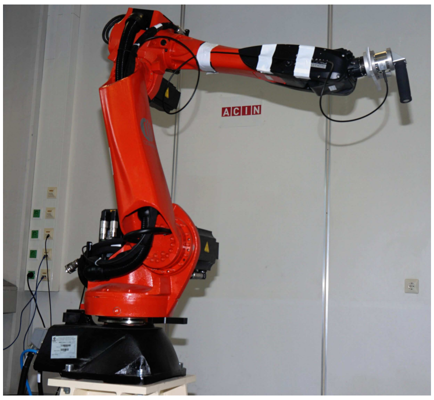

Fig. 4. Six-axis industrial robot.

on a six-axis industrial robot. Thereby, the control laws (17), (19), and (23) are used to stabilize the robot on a paraboloid of revolution. The operator is able to move the robot along the surface without effort by using low stiffness $k_{||}^d$ and damping $d_{||}^d$ in tangential direction. The stiffness $k_{\perp}^d$ and damping $d_{\perp}^d$ in orthogonal direction are chosen rather high to limit the deviations from the surface. To avoid representation singularities of the orientation, the compliance control laws (25) and (26) are utilized to compute the new orientation input $\mathbf{v}_{s,o}$. The control parameters for (19) and (26) are listed in Tab. III and the impedance parameters in Tab. IV.

TABLE III
CONTROLLER PARAMETERS FOR DYNAMIC SFC/PFC.

Symbol	Value	Unit	Symbol	Value	Unit
$a_{\eta,0}$	4913	$1/\mathrm{s}^3$	$a_{\xi,0}$	17576	$1/\mathrm{s}^3$
$a_{\eta,1}$	867	$1/\mathrm{s}^2$	$a_{\xi,1}$	2028	$1/\mathrm{s}^2$
$a_{\eta,2}$	51	$1/\mathrm{s}$	$a_{\xi,2}$	78	$1/\mathrm{s}$
$a_{o,1}$	2700	$1/\mathrm{s}^2$	$a_{o,2}$	90	$1/\mathrm{s}$

Note that this experiment is equal to an implementation of soft guidance virtual fixtures on a surface.

A. System

The six-axis industrial robot of Fig. 4 is used for the experiment. Its Denavit-Hartenberg parameters are listed in Tab. V and its maximum payload is given by 7kg.

The 6D-force/torque sensor $K6\text{-}D40$ from ME-MESSSYSTEME is attached to the robot's end-effector

TABLE IV
COMPLIANCE CONTROL PARAMETERS FOR DYNAMIC SFC/PFC.

Symbol	Value	Unit	Symbol	Value	Unit
$m_{\|\|}^d$	3	kg	$m_{\perp}^d$	3	kg
$d_{\|\|}^d$	90	$\mathrm{Ns/m}$	$d_{\perp}^d$	150	$\mathrm{Ns/m}$
$k_{\|\|}^d$	1.5	$\mathrm{N/m}$	$k_{\perp}^d$	5	$\mathrm{kN/m}$
m_r^d	0.2	kgm^2	k_r^d	34.4	$\mathrm{Nm/rad}$
d_r^d	24.6	$\mathrm{Nms/rad}$			

Post-print version of the article: B. Bischof, T. Glück, M. Böck, and A. Kugi, "A path/surface following control approach to generate virtual fixtures", *IEEE Transactions on Robotics*, vol. 34, no. 6, pp. 1577–1592, 2018, ISSN: 1552-3098. DOI: 10.1109/TRO.2018.2861913
The content of this post-print version is identical to the published paper but without the publisher's final layout or copy editing.

TABLE V
DH PARAMETERS OF THE INDUSTRIAL ROBOT.

i	d_i	a_i	α_i	i	d_i	a_i	α_i
1	$0.43m$	$0.15m$	$\frac{\pi}{2}$	4	$0.684m$	0	$-\frac{\pi}{2}$
2	0	$0.59m$	0	5	0	0	$\frac{\pi}{2}$
3	0	$0.13m$	$\frac{\pi}{2}$	6	$0.1m$	0	0

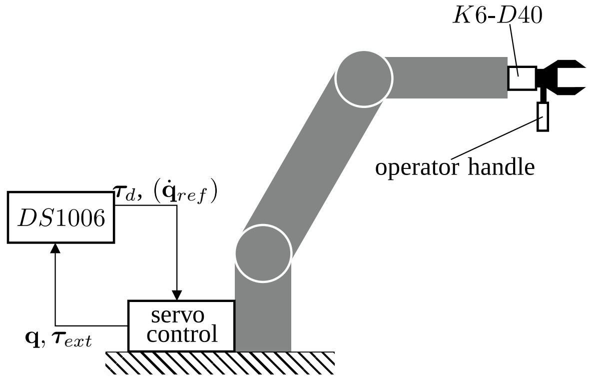

Fig. 5. Experimental setup.

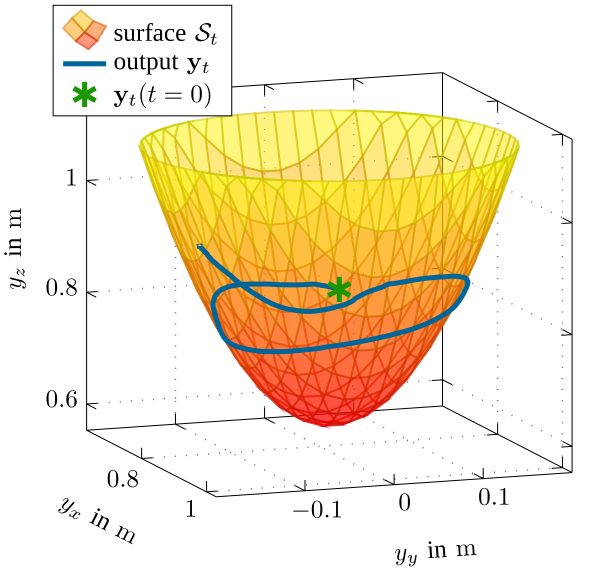

Fig. 6. Surface $\mathcal{S}_t$ and measured output $\mathbf{y}_t$ of the dynamic SFC experiment.

and used as haptic input device. The dynamic parameters including Coulomb and viscous friction are identified using linear regression methods described in [30] and [31].

The dynamic SFC is implemented on the real-time system $DS1006$ from DSPACE with a sampling time of $T_s = 1\,\mathrm{ms}$ and the torque commands $\boldsymbol{\tau}_d$ are sent to joint servo controllers. The experimental setup is depicted in Fig. 5. Newton's method is applied to solve the optimization problem (4) numerically. The numerical integration (7) is implemented using the explicit Euler method.

B. Measurement Results of the Dynamic SFC

The surface $\mathcal{S}$ is defined as a paraboloid of revolution with constant orientation using the smooth parametrization

$$\boldsymbol{\sigma}(\boldsymbol{\theta}) = \begin{bmatrix} \boldsymbol{\sigma}_t(\boldsymbol{\theta}) \\ \boldsymbol{\sigma}_r \end{bmatrix} = \begin{bmatrix} (\theta_1 + 0.83)\mathrm{m} \\ (\theta_2)\mathrm{m} \\ (12.5(\theta_1^2 + \theta_2^2) + 0.6)\mathrm{m} \\ 0 \\ \pi/4 \\ \pi - 0.1 \end{bmatrix} \tag{36}$$

and is depicted in Fig 6.

The external references $\boldsymbol{\eta}_1^d$ and ξ_1^d are set to zero. Hence, the robot's motion is only caused by the input forces of the operator via the impedance control law (23) and is depicted in Fig. 6. Fig. 7(a) shows that the desired motion on the surface $\boldsymbol{\eta}_1^p = [\eta_{1,1}^p \; \eta_{1,2}^p]^{\mathrm{T}}$ is tracked very well. The desired deviation from the surface $\mathcal{S}_t$ corresponds with the operator's input force in orthogonal direction $\tau_\perp$, cf. Fig. 7(b) and Fig. 7(c). An operator force of less than 20N is necessary for the motion along the surface. Fig. 7(d) and Fig. 7(e) show that the impedance of the orientation behaves as specified. The first three joint torques are depicted in Fig. 7(f).

Hence, the results of this experiment confirm that the proposed SFC approach is well suited to be combined with compliance control.

V. VIRTUAL FIXTURE IMPLEMENTATION EXAMPLES

This section presents four additional implementation examples of virtual fixtures generated with PFC/SFC. For this, the experimental setup of Section IV-A is used. These examples comprise the following virtual fixtures:

Example 1: Static guidance virtual fixtures on a path with soft constraints

Example 2: Static guidance virtual fixtures on a path with hard constraints

Example 3: Dynamic guidance virtual fixtures on a path with hard constraints

Example 4: Static forbidden region virtual fixtures with hard constraints

PFC and SFC are implemented on the real-time system $DS1006$ from DSPACE with a sampling time of $T_s = 1\,\mathrm{ms}$ and the torque commands $\boldsymbol{\tau}_d$ are sent to joint servo controllers. When the kinematic PFC/SFC is used, the reference joint velocities $\dot{\mathbf{q}}_{\mathrm{ref}}$ are transferred to the servo controller instead of the torques. For details on the implementation, the reader is referred to [17].

The operator does not have any optical feedback about the path/surface or the deviation from the path/surface during the experiments.

A. Example 1: Static guidance virtual fixtures on a path with soft constraints

Guidance virtual fixtures on a path γ with soft constraints are generated by a combination of the dynamic PFC (39) with compliance control (42) and (41). The robot's end-effector is supposed to move on a horizontal circle with radius

Post-print version of the article: B. Bischof, T. Glück, M. Böck, and A. Kugi, "A path/surface following control approach to generate virtual fixtures", *IEEE Transactions on Robotics*, vol. 34, no. 6, pp. 1577–1592, 2018, ISSN: 1552-3098. DOI: 10.1109/TRO.2018.2861913
The content of this post-print version is identical to the published paper but without the publisher's final layout or copy editing.

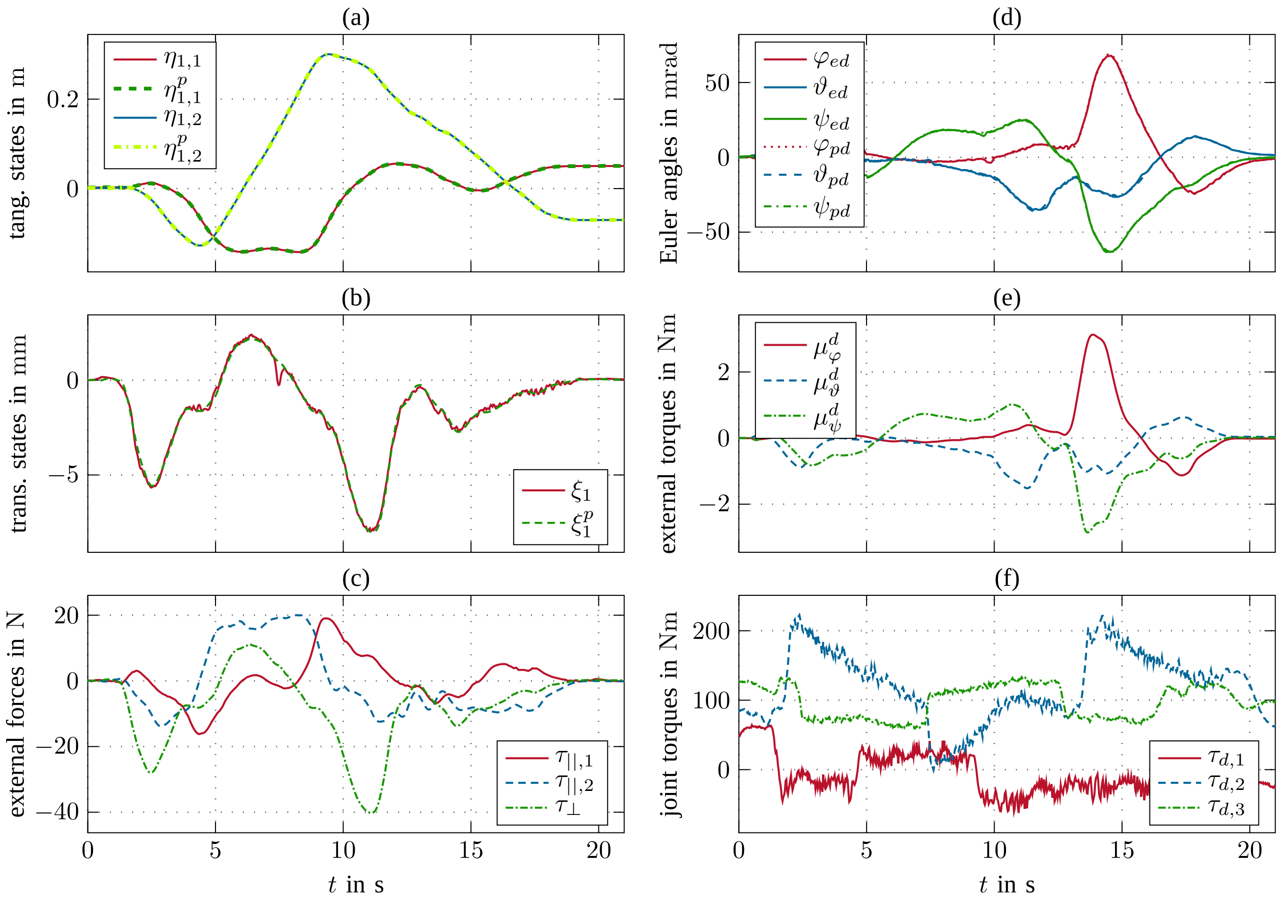

Fig. 7. Experimental results of the dynamic SFC validation.

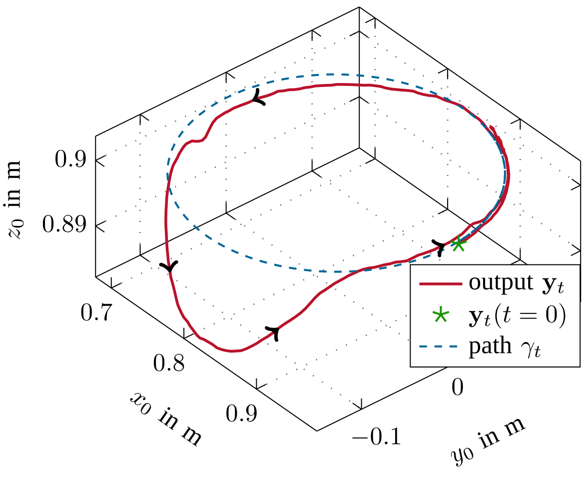

Fig. 8. Path γ_t and output $\mathbf{y}_t$ with soft guidance virtual fixtures (Example 1).

$r_{pc} = 0.15$m and center $\mathbf{y}_{pc}^{\mathrm{T}} = [0.83\ 0\ 0.9]$m and the constant orientation $\boldsymbol{\sigma}_r^{\mathrm{T}} = [0, \pi/4, \pi - 0.1]$rad, cf. Fig. 8.

A low stiffness $k_{||}^d$ and damping $d_{||}^d$ in tangential direction enable the operator to move the robot along the circle without effort. The stiffness $k_\perp^d$ and damping $d_\perp^d$ in orthogonal direction are chosen rather high to limit the deviations from the path. The orientation is also made compliant with respect to $\boldsymbol{\sigma}_r$ by applying the control law (26) for the input $\mathbf{v}_{p,o}$. The control parameters for (26) and (41) are listed in Tab. III and the impedance parameters in Tab. IV. The external references η_1^d, ξ_1^d, and ξ_3^d are set to zero. For a free motion along the path γ, the tangential stiffness $k_{||}^d$ can be set to zero. In the following experiments, however, $k_{||}^d$ is set to a very low stiffness to limit the drift along the path resulting from force sensor bias.

In the experiment, the operator moves the robot along the circle for approximately $1\frac{1}{4}$ revolutions. In the middle of the experiment, the robot is pushed down in negative z_0-direction to deviate considerably from the path, cf. Fig. 8.

Fig. 9(a) shows that the arc length on the circle η_1 follows the reference η_1^p, which is the output of the impedance control law (42a). The robot deviates from the circle corresponding to the external forces. This gets clear by comparing the transversal states ξ_1^p and ξ_3^p in Fig. 9(b) with the external forces $\tau_\perp$ and $\tau_\pitchfork$ in Fig. 9(c). The deviations of ξ_i from ξ_i^p, $i = 1, 3$, mainly occur at joint velocity zero crossings and are caused by uncompensated friction effects.

The rotational coordinates, the external torques as well as

Post-print version of the article: B. Bischof, T. Glück, M. Böck, and A. Kugi, "A path/surface following control approach to generate virtual fixtures", *IEEE Transactions on Robotics*, vol. 34, no. 6, pp. 1577–1592, 2018, ISSN: 1552-3098. DOI: 10.1109/TRO.2018.2861913
The content of this post-print version is identical to the published paper but without the publisher's final layout or copy editing.

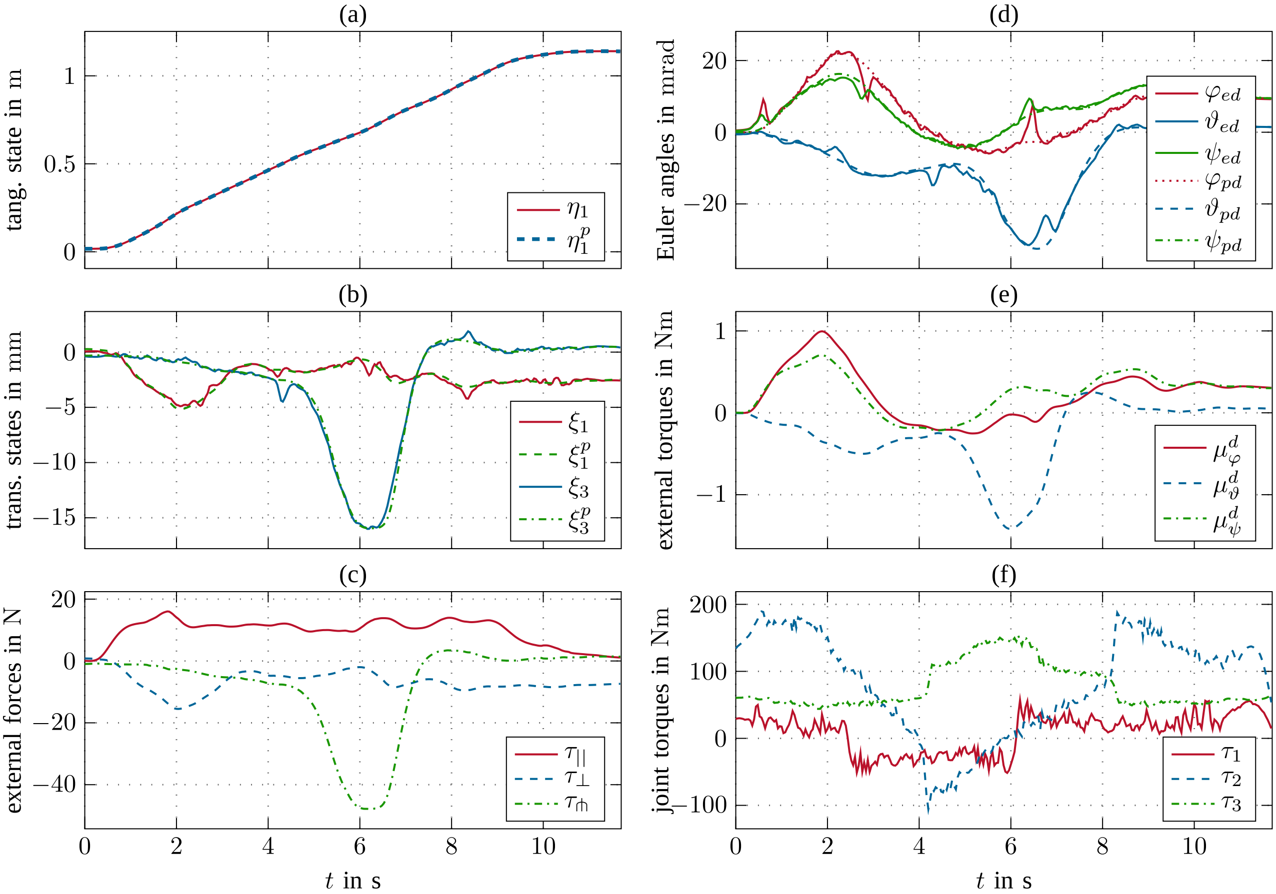

Fig. 9. Experimental results for soft guidance virtual fixtures (Example 1).

the first three joint torques are depicted in Fig. 9(d), Fig. 9(e), and Fig. 9(f), respectively. The Euler angles φ_{pd}, ϑ_{pd}, and ψ_{pd} represent the desired deviation from the reference orientation $\boldsymbol{\sigma}_r$, which is caused by the external torques μ^d_φ, μ^d_ϑ, and μ^d_ψ. Again, errors between the actual deviation φ_{ed}, ϑ_{ed}, and ψ_{ed} and the reference deviation φ_{pd}, ϑ_{pd}, and ψ_{pd} mainly occur at joint velocity zero crossings.

B. Example 2: Static guidance virtual fixtures on a path with hard constraints

In this implementation example, the kinematic PFC (43) with the position controller (45) and the analytic Jacobian $\mathbf{J}_a$ (49) in (38) is used to restrict the robot's motion to a path. Additionally, the impedance control (42a) for the tangential direction, with parameters $m^d_{||}$, $d^d_{||}$, and $k^d_{||}$ from Tab. IV, allows the operator to move the robot along the path without effort. Hard constraints are ensured by setting the references for the transversal states ξ^p_1 and ξ^p_3 as well as their derivatives to zero. The orientation is also made stiff by setting the reference to $(\mathbf{y}^p_r)^{\mathrm{T}} = \boldsymbol{\sigma}^{\mathrm{T}}_r(\theta^*) = [\varphi_p \ \vartheta_p \ \psi_p]$. Tab. VI lists the control parameters. The path γ is defined by cubic splines and its position part γ_t is depicted in Fig. 10. The operator moves the robot from the beginning of the spline path until the end and then backwards again, cf. Fig. 11(a). During the backwards motion, a considerable force is applied in normal direction to the path, which can be seen in Fig. 11(c). Fig. 11(b) shows that the robot remains on the path with deviations of less than 0.4mm. The orientation of the end-effector $\mathbf{y}^{\mathrm{T}}_r = [\varphi_e \ \vartheta_e \ \psi_e]$ follows the reference orientation $\boldsymbol{\sigma}_r(\theta^*)$ without notable errors even with applied external torques, cf. Fig. 11(d).

C. Example 3: Dynamic guidance virtual fixtures on a path with hard constraints

The same control law of Section V-B and path of Section V-A with constant orientation $\boldsymbol{\sigma}^{\mathrm{T}}_r = [0, \pi/4, \pi - 0.1]$rad are employed in this implementation example, but now, the radius of the circle is a function of time and given by $r_p(t) = r_{pc} + a_{rp}\sin(2\pi f_{rp} t)$, with $a_{rp} = 20$mm and $f_{rp} = 0.5$Hz.

TABLE VI
CONTROLLER PARAMETERS FOR KINEMATIC PFC.

Symbol	Value	Unit	Symbol	Value	Unit
a_η	10	1/s	a_ξ	15	1/s
a_r	12	1/s			

Post-print version of the article: B. Bischof, T. Glück, M. Böck, and A. Kugi, "A path/surface following control approach to generate virtual fixtures", *IEEE Transactions on Robotics*, vol. 34, no. 6, pp. 1577–1592, 2018, ISSN: 1552-3098. DOI: 10.1109/TRO.2018.2861913
The content of this post-print version is identical to the published paper but without the publisher's final layout or copy editing.

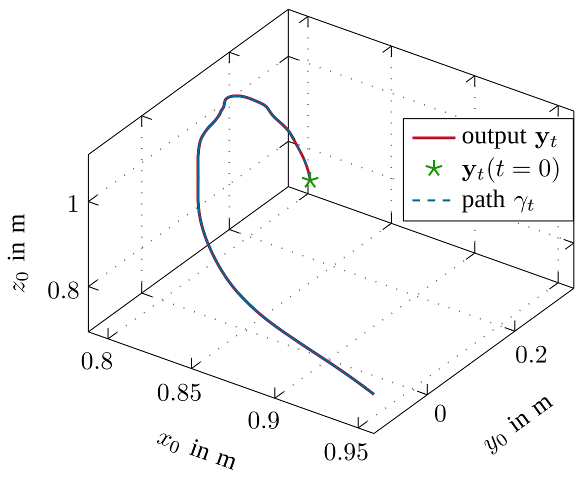

Fig. 10. Path γ_t and output $\mathbf{y}_t$ with hard guidance virtual fixtures (Example 2).

Hence, the radius of the circle constraint oscillates between $r_{p,min} = 0.13$m and $r_{p,max} = 0.17$m with a period of 2s and $\Delta\boldsymbol{\sigma}_t^{\mathrm{T}}(t) = a_{rp}\sin(2\pi f_{rp}t)\,[\cos(\theta)\;\sin(\theta)\;0]$. The impedance control (42a) for the tangential direction, with parameters from Tab. IV, allows the operator to move the robot along the path without effort.

Hard constraints and dynamic virtual fixtures are implemented by setting the references for the transversal states to $\xi_1^p = \mathbf{e}_\perp^{\mathrm{T}}\Delta\boldsymbol{\sigma}_t = a_{rp}\sin(2\pi f_{rp}t)$ and $\xi_3^p = \mathbf{e}_\pitchfork^{\mathrm{T}}\Delta\boldsymbol{\sigma}_t = 0$. The PFC control parameters are listed in Tab. VI.

In this implementation example, the operator moves the robot along the oscillating circle for almost one revolution. The velocity of the robot along the circle is increased during the experiment to show the time dependency of the virtual fixture, cf. Fig. 12, where the circles with the minimum and maximum radius, $r_{p,\min}$ and $r_{p,\max}$, as well as the robot's end-effector position $\mathbf{y}_t$ in the horizontal plane are depicted.

Fig. 13 shows the tangential, transversal states, the external forces, and the torques of the first three motors. The transversal reference ξ_1^p oscillates at 0.5Hz with an amplitude of 20mm and the state ξ_1 follows without noticeable errors, cf. Fig. 13(b).

D. Example 4: Static forbidden region virtual fixtures with hard constraints

Forbidden region virtual fixtures with hard constraints are implemented in this experiment. The robot's motion is restricted to a cylinder with radius $r_{cy} = 0.2$m, height $h_{cy} = 0.4$m, and vertical rotation axis with the coordinates $x_{ra} = 0.9$m and $y_{ra} = 0$. Additionally, a paraboloid of revolution with height $h_{pr} = 0.2$m, radius $r_{pr} = 0.076$m, and rotation axis coordinates $x_{pr} = 0.95$m and $y_{pr} = 0$ further restricts the workspace inside the cylinder, cf. Fig. 14. A Cartesian position-based impedance control [23], [28] (often denoted as Cartesian admittance control) is used to enable an unconstrained movement of the manipulator inside the feasible region of the restricted workspace. Thereby, the parameters $m_{||}^d$, $k_{||}^d$, and $d_{||}^d$ from Tab. IV are used.

Once a limiting surface is reached, kinematic SFC (29) with position control (31) and $\xi_1^p \equiv 0$ is activated to prevent the robot from entering the forbidden region. The impedance control law (23a) is used to compute the two elements of the reference $\boldsymbol{\eta}_1^p$ with parameters from Tab. IV.

Kinematic PFC (43) with the controller (45) gets active when the robot reaches the intersection of the two surfaces, i.e., a plane intersects the cylinder or the paraboloid of revolution, hence, the path is a circle with radius r_{cy} or r_{pr}. Additionally, the impedance control (42a) for the tangential direction, with parameters from Tab. IV, allows the operator to move the robot along the path without effort. Admittance control (AdmC) gets active again once the intended motion from the operator points away from the forbidden region.

Continuous tangential velocities at the transitions are ensured by setting the initial tangential references to $\dot{\boldsymbol{\eta}}_1^p(t_{\mathrm{switch}}) = [\mathbf{I}\;\;\mathbf{0}]\hat{\mathbf{J}}_s\dot{\mathbf{q}}(t_{\mathrm{switch}})$ and $\dot{\eta}_1^p(t_{\mathrm{switch}}) = [1\;\;\mathbf{0}]\hat{\mathbf{J}}_p\dot{\mathbf{q}}(t_{\mathrm{switch}})$, respectively. The analytic Jacobian $\mathbf{J}_a$ is used for the PFC (43) and SFC (29). Tab. VII lists the control parameters.

TABLE VII
CONTROLLER PARAMETERS FOR KINEMATIC PFC/SFC.

Symbol	Value	Unit	Symbol	Value	Unit
a_η	5	1/s	a_ξ	5	1/s
a_r	12	1/s			

In the experiment, the robot starts inside the feasible area at point $\mathbf{y}_{t,0}^{\mathrm{T}} = [1.094\;0.02\;1.077]$m, which is marked with an asterisk in Fig. 14. AdmC is activated and the operator moves the robot towards the paraboloid of revolution (path A). Once the paraboloid of revolution is reached, SFC gets enabled to prevent the robot from entering the forbidden region (path B). AdmC gets active once the input force of the operator points away from the surface of the paraboloid of revolution. Now, the operator moves the robot towards the cylinder (path C). SFC gets enabled again when the surface of the cylinder is reached and the operator moves the robot along the cylinder towards the lower vertical limit $z_{0,\min} = 0.7$m (path D). When the lower vertical limit is reached, PFC on a circle with radius r_{cy} gets active because the operator's intended motion points in negative z_0 direction and to the outside of the cylinder (path E). The operator's input force then points into the inside of the cylinder and SFC on the xy-plane with $z_{0,\min}$ is enabled (path F). On the last path segment, the robot is moved in positive z_0-direction with AdmC (path G).

Fig. 15 shows the tangential states, the transversal state, the external forces, and the first three motor torques of the motion along the cylinder with SFC (path D). The first tangential state $\eta_{1,1}$ represents the arc length of the trajectory projected on the xy-plane and the second tangential state $\eta_{1,2}$ represents the z-component of the trajectory. The transversal state ξ_1 represents the deviation from the cylinder, where negative values are a

Post-print version of the article: B. Bischof, T. Glück, M. Böck, and A. Kugi, "A path/surface following control approach to generate virtual fixtures", *IEEE Transactions on Robotics*, vol. 34, no. 6, pp. 1577–1592, 2018, ISSN: 1552-3098. DOI: 10.1109/TRO.2018.2861913
The content of this post-print version is identical to the published paper but without the publisher's final layout or copy editing.

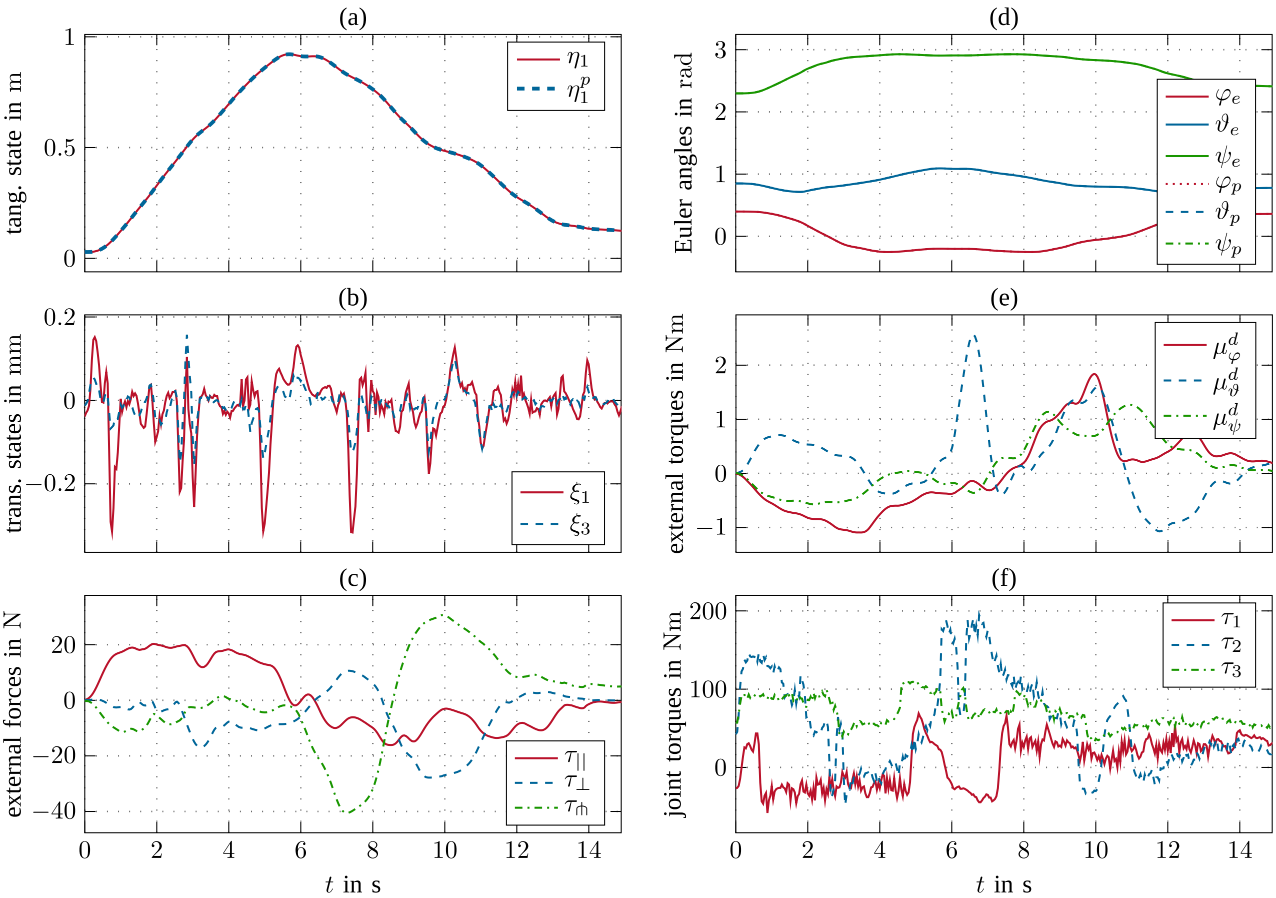

Fig. 11. Experimental results for hard guidance virtual fixtures (Example 2).

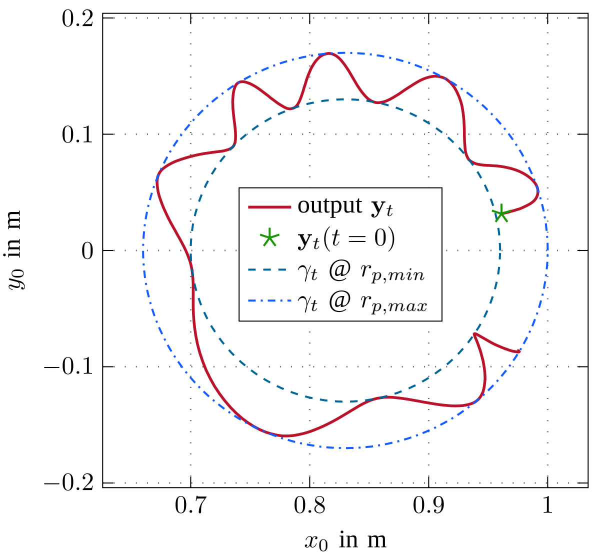

Fig. 12. Path γ_t with the time varying radius $r_p(t) = r_{pc} + a_{rp} \sin(2\pi f_{rp} t)$ and output $\mathbf{y}_t$ with dynamic virtual fixtures (Example 3).

penetration of the forbidden region. Hence, the penetration is less than 0.2mm.

VI. Conclusions

This paper introduced a combination of surface following control (SFC) with compliance control and presented a path following control (PFC) and SFC approach to generate virtual fixtures for physical human-robot interaction. This approach allows to systematically implement a large number of different constraint types like guidance and forbidden region virtual fixtures, hard and soft constraints as well as static and dynamic virtual fixtures and their combinations. The ability to use splines for the path and surface definition enables a high flexibility for the geometry of the virtual fixtures. Guidance virtual fixtures with hard or soft constraints can simply be generated in a straightforward manner with PFC or SFC. Forbidden region virtual fixtures require more implementation and computational effort, because the distance to each surface in the unconstrained motion state and to each intersection path in the SFC state has to be calculated in every sampling instance to ensure a proper switching between the control states. A more efficient method to find the closest surface could be part of future research as well as dynamic forbidden region virtual fixtures and forbidden region virtual fixtures with soft

Post-print version of the article: B. Bischof, T. Glück, M. Böck, and A. Kugi, "A path/surface following control approach to generate virtual fixtures", *IEEE Transactions on Robotics*, vol. 34, no. 6, pp. 1577–1592, 2018, ISSN: 1552-3098. DOI: 10.1109/TRO.2018.2861913
The content of this post-print version is identical to the published paper but without the publisher's final layout or copy editing.

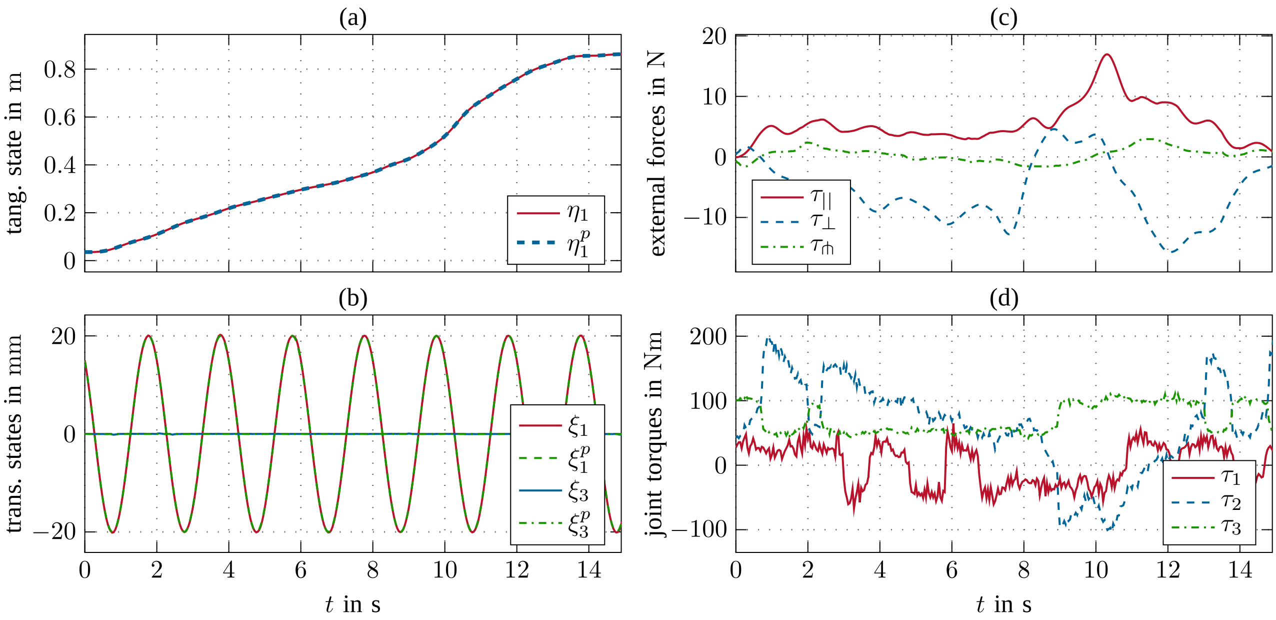

Fig. 13. Experimental results for hard guidance dynamic virtual fixtures (Example 3).

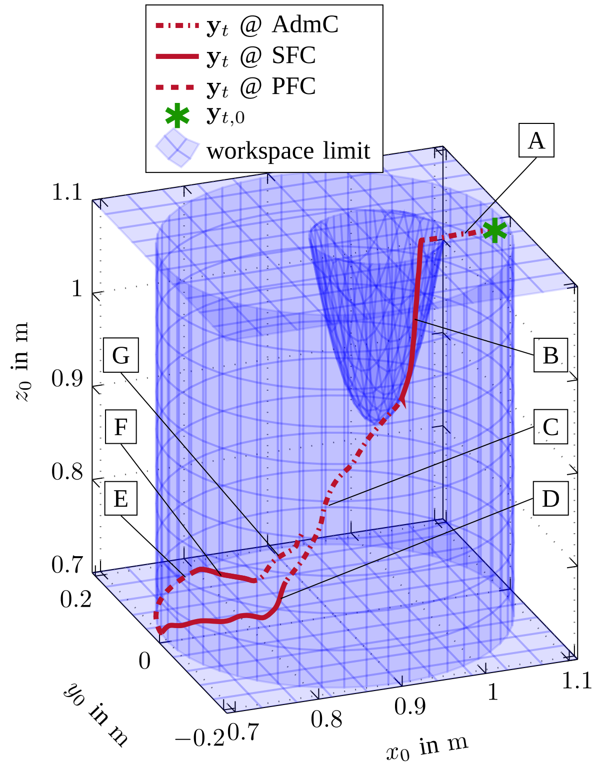

Fig. 14. Forbidden region and measured output $\mathbf{y}_t$ (Example 4).

constraints. For a verification of the method, five different experiments on an industrial robot were performed and show very good results.

Appendix A
Path Following Control

In this section, the PFC control law of [17] for the dynamic system (1) is shortly revisited and the simplification for the kinematic model (3) is introduced.

A. Dynamic Path Following Control (dynamic PFC)

The tangential coordinate η_1 for the PFC is defined as the arc length of a path γ_t and the transversal coordinates ξ_1 and ξ_3 are defined as the projection of the shortest distance to the path onto the normal vectors $\mathbf{e}_{\perp}$ and $\mathbf{e}_{\pitchfork}$, respectively. The vectors $\mathbf{e}_{||}(\theta)$, $\mathbf{e}_{\perp}(\theta)$, and $\mathbf{e}_{\pitchfork}(\theta)$ span an orthonormal parallel transport frame to the path γ_t at $\boldsymbol{\sigma}_t(\theta)$, where θ denotes the path parameter and $\mathbf{e}_{||}(\theta)$ the tangential unit vector. We introduce the virtual output $\hat{\mathbf{y}}_p^{\mathrm{T}} = \hat{\mathbf{h}}_p^{\mathrm{T}}(\mathbf{q}) = [\eta_1, \xi_1, \xi_3, \boldsymbol{\zeta}^{\mathrm{T}}]$. Its time-derivative is given by

$$\dot{\hat{\mathbf{y}}}_p = \mathbf{L}_p(\mathbf{q})\dot{\mathbf{y}} = \hat{\mathbf{J}}_p(\mathbf{q})\dot{\mathbf{q}} \ , \tag{37}$$

with the PFC Jacobian

$$\hat{\mathbf{J}}_p(\mathbf{q}) = \mathbf{L}_p(\mathbf{q})\mathbf{J}(\mathbf{q}) \tag{38}$$

and the matrices

$$\mathbf{L}_p(\mathbf{q}) = \begin{bmatrix} \mathbf{E}_p(\mathbf{q}) & \mathbf{0} \\ \mathbf{0} & \mathbf{I} \end{bmatrix} \quad \text{and} \quad \mathbf{E}_p(\mathbf{q}) = \begin{bmatrix} \beta(\mathbf{y}_t)\mathbf{e}_{||}^{\mathrm{T}} \\ \mathbf{e}_{\perp}^{\mathrm{T}} \\ \mathbf{e}_{\pitchfork}^{\mathrm{T}} \end{bmatrix} ,$$

where the scalar $\beta(\mathbf{y}_t)$ depends on the distance to the path and $\beta(\mathbf{y}_t = \boldsymbol{\sigma}_t) = 1$ holds, cf. [17].

Application of the feedback transformation, see [17],

$$\boldsymbol{\tau}_d = \mathbf{n}(\mathbf{q}, \dot{\mathbf{q}}) - \boldsymbol{\tau}_{ext} + \mathbf{D}(\mathbf{q})\hat{\mathbf{J}}_p^{-1}(\mathbf{q})\big(\mathbf{v} - \dot{\hat{\mathbf{J}}}_p(\mathbf{q}, \dot{\mathbf{q}})\dot{\mathbf{q}}\big) \tag{39}$$

to the system (1) with output function (2) results in a linear input-output relation from the new control input $\mathbf{v}_p^{\mathrm{T}} =$

Post-print version of the article: B. Bischof, T. Glück, M. Böck, and A. Kugi, "A path/surface following control approach to generate virtual fixtures", *IEEE Transactions on Robotics*, vol. 34, no. 6, pp. 1577–1592, 2018, ISSN: 1552-3098. DOI: 10.1109/TRO.2018.2861913
The content of this post-print version is identical to the published paper but without the publisher's final layout or copy editing.

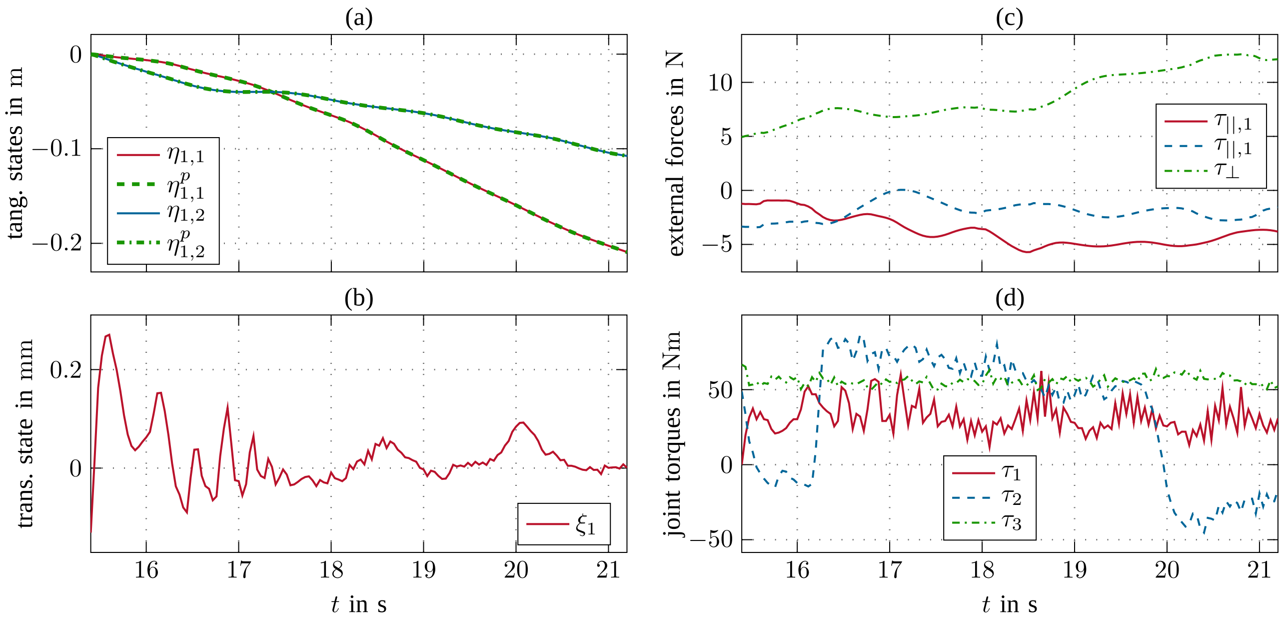

Fig. 15. Experimental results for forbidden region virtual fixtures for the path segment D in Fig. 14 (Example 4).

$[\mathbf{v}^{\mathrm{T}}_{p,t} \quad \mathbf{v}^{\mathrm{T}}_{p,r}]$, where $\mathbf{v}^{\mathrm{T}}_{p,t} = [v_{||} \quad v_\perp \quad v_\pitchfork]$ to the virtual output $\hat{\mathbf{y}}_p$ in the form of m integrator chains of length two

$$\ddot{\hat{\mathbf{y}}}_p = \mathbf{v}_p \ . \tag{40}$$

The position control law

$$\mathbf{v}_p = \begin{bmatrix} \mathbf{v}_{p,t} \\ \mathbf{v}_{p,r} \end{bmatrix} = \begin{bmatrix} \ddot{\eta}^p_1 - a_{\eta,2}\dot{e}^p_\eta - a_{\eta,1}e^p_\eta \\ \ddot{\xi}^p_1 - a_{\xi,2}\dot{e}^p_{\xi_1} - a_{\xi,1}e^p_{\xi_1} \\ \ddot{\xi}^p_3 - a_{\xi,2}\dot{e}^p_{\xi_3} - a_{\xi,1}e^p_{\xi_3} \\ \ddot{\mathbf{y}}^p_r - a_{r,2}\dot{\mathbf{e}}^p_r - a_{r,1}\mathbf{e}^p_r \end{bmatrix} , \tag{41}$$

where $e^p_\eta = \eta_1 - \eta^p_1$, $e^p_{\xi_1} = \xi_1 - \xi^p_1$, $e^p_{\xi_3} = \xi_3 - \xi^p_3$, and $\mathbf{e}^p_r = \mathbf{y}_r - \mathbf{y}^p_r$, yields an exponentially stable error dynamics, if $a_{i,j} > 0$ with $i \in \{\eta, \xi, r\}$ and $j = 1, 2$. The reference position on the path is denoted by η^p_1 and the references for the orthogonal states by ξ^p_1 and ξ^p_3. The reference for the orientation is given by $\mathbf{y}^p_r = \boldsymbol{\sigma}_r(\theta^*)$.

Using the position controller (45) and assuming perfect tracking, the impedance control law follows as

$$\begin{aligned} \ddot{\eta}^p_1 &= \ddot{\eta}^d_1 + \frac{\tau_{||}}{m^d_{||}} - \frac{d^d_{||}}{m^d_{||}}\dot{e}^{pd}_\eta - \frac{k^d_{||}}{m^d_{||}}e^{pd}_\eta , \\ \dot{\eta}^p_1 &= \int_0^t \ddot{\eta}^p_1 \mathrm{d}\tau, \quad \eta^p_1 = \int_0^t \dot{\eta}^p_1 \mathrm{d}\tau , \end{aligned} \tag{42a}$$

$$\begin{aligned} \ddot{\xi}^p_1 &= \ddot{\xi}^d_1 + \frac{\tau_\perp}{m^d_\perp} - \frac{d^d_\perp}{m^d_\perp}\dot{e}^{pd}_{\xi_1} - \frac{k^d_\perp}{m^d_\perp}e^{pd}_{\xi_1} , \\ \dot{\xi}^p_1 &= \int_0^t \ddot{\xi}^p_1 \mathrm{d}\tau, \quad \xi^p_1 = \int_0^t \dot{\xi}^p_1 \mathrm{d}\tau , \end{aligned} \tag{42b}$$

$$\begin{aligned} \ddot{\xi}^p_3 &= \ddot{\xi}^d_3 + \frac{\tau_\perp}{m^d_\perp} - \frac{d^d_\perp}{m^d_\perp}\dot{e}^{pd}_{\xi_3} - \frac{k^d_\perp}{m^d_\perp}e^{pd}_{\xi_3} , \\ \dot{\xi}^p_3 &= \int_0^t \ddot{\xi}^p_3 \mathrm{d}\tau, \quad \xi^p_3 = \int_0^t \dot{\xi}^p_3 \mathrm{d}\tau , \end{aligned} \tag{42c}$$

with $\mathbf{y}^p_r$ from (23c) and the errors $e^{pd}_\eta = \eta^p_1 - \eta^d_1$ and $e^{pd}_{\xi_3} = \xi^p_3 - \xi^d_3$. The same approach as described for dynamic SFC can be used to avoid singularities in the case of $\mathbf{y}_r \in \mathbb{R}^3$.

B. Kinematic Path Following Control (kinematic PFC)

As in SFC, the PFC control law can also be drastically simplified when ideal subordinate velocity controllers are employed, see (3). Because of the relation (37), application of the feedback transformation

$$\dot{\mathbf{q}}_{\mathrm{ref}} = \hat{\mathbf{J}}^{-1}_p \mathbf{v}_{p,k} \tag{43}$$

to the system (3), with the new control input $\mathbf{v}^{\mathrm{T}}_{p,k} = [\mathbf{v}^{\mathrm{T}}_{p,k,t} \ \mathbf{v}^{\mathrm{T}}_{p,k,r}]$, where $\mathbf{v}^{\mathrm{T}}_{p,k,t} = [v_{k,||} \ v_{k,\perp} \ v_{k,\pitchfork}]$, results in a linear input-output relation from the new control input $\mathbf{v}_{p,k}$ to the virtual PFC output $\hat{\mathbf{y}}_p$ in the form of m integrator chains

$$\dot{\hat{\mathbf{y}}}_p = \mathbf{v}_{p,k} \ . \tag{44}$$

The position control law

$$\mathbf{v}_{p,k} = \begin{bmatrix} \mathbf{v}_{p,k,t} \\ \mathbf{v}_{p,k,r} \end{bmatrix} = \begin{bmatrix} \dot{\eta}^p_1 - a_\eta e^p_\eta \\ \dot{\xi}^p_1 - a_\xi e^p_{\xi_1} \\ \dot{\xi}^p_3 - a_\xi e^p_{\xi_3} \\ \dot{\mathbf{y}}^p_r - a_r \mathbf{e}^p_r \end{bmatrix} , \tag{45}$$

yields an exponentially stable error dynamics, if $a_i > 0$ with $i \in \{\eta, \xi, r\}$.

The impedance control law to compute the references η^p_1, ξ^p_1, ξ^p_3, and $\mathbf{y}^p_r$ is identical to the dynamic PFC and given by (42).

Post-print version of the article: B. Bischof, T. Glück, M. Böck, and A. Kugi, "A path/surface following control approach to generate virtual fixtures", *IEEE Transactions on Robotics*, vol. 34, no. 6, pp. 1577–1592, 2018, ISSN: 1552-3098. DOI: 10.1109/TRO.2018.2861913
The content of this post-print version is identical to the published paper but without the publisher's final layout or copy editing.

Appendix B
Geometric and Analytic Jacobian

The relationship between the angular velocity of the end-effector $\boldsymbol{\omega}_e$ expressed in the inertial frame and the time-derivative of the Euler angles $\dot{\boldsymbol{\phi}}_e$ given in ZYX convention $\boldsymbol{\phi}_e^{\mathrm{T}} = \begin{bmatrix} \varphi & \vartheta & \psi \end{bmatrix}$ reads as, see [26],

$$\boldsymbol{\omega}_e = \mathbf{T}(\boldsymbol{\phi}_e)\dot{\boldsymbol{\phi}}_e \tag{46}$$

with

$$\mathbf{T}(\boldsymbol{\phi}_e) = \begin{bmatrix} 0 & -\sin(\varphi) & \cos(\varphi)\cos(\vartheta) \\ 0 & \cos(\varphi) & \sin(\varphi)\cos(\vartheta) \\ 1 & 0 & -\sin(\vartheta) \end{bmatrix} . \tag{47}$$

We now have to distinguish between the manipulator (geometric) Jacobian $\mathbf{J}_g$ and the analytic Jacobian $\mathbf{J}_a$, where

$$\begin{bmatrix} \dot{\mathbf{y}}_t \\ \boldsymbol{\omega}_e \end{bmatrix} = \mathbf{J}_g \dot{\mathbf{q}} \tag{48}$$

and

$$\begin{bmatrix} \dot{\mathbf{y}}_t \\ \dot{\boldsymbol{\phi}}_e \end{bmatrix} = \mathbf{J}_a \dot{\mathbf{q}} \tag{49}$$

holds, with the analytic Jacobian

$$\mathbf{J}_a = \begin{bmatrix} \mathbf{I} & \mathbf{0} \\ \mathbf{0} & \mathbf{T}^{-1}(\boldsymbol{\phi}_e) \end{bmatrix} \mathbf{J}_g . \tag{50}$$

References

[1] B. Gillespie, E. Colgate, and M. Peshkin, "A general framework for cobot control," *IEEE Transactions on Robotics and Automation*, vol. 17, no. 4, pp. 391–401, 2001.

[2] J. Abbott, P. Marayong, and A. Okamura, "Haptic virtual fixtures for robot-assisted manipulation," in *Robotics research*, S. Thrun, R. Brooks, and H. Durrant-Whyte, Eds. Berlin Heidelberg: Springer, 2007, pp. 49–64.

[3] P. Akella, M. Peshkin, E. Colgate, W. Wannasuphoprasit, N. Nagesh, J. Wells, S. Holland, T. Pearson, and B. Peacock, "Cobots for the automobile assembly line," in *Proceedings of the IEEE International Conference on Robotics and Automation*, Detroit, Michigan, USA, May 1999, pp. 728–733.

[4] A. Bicchi, M. Peshkin, and E. Colgate, "Safety for physical human-robot interaction," in *Springer handbook of robotics*, B. Siciliano and O. Khatib, Eds. Berlin Heidelberg: Springer, 2008, pp. 1335–1348.

[5] M. Peshkin, E. Colgate, W. Wannasuphoprasit, C. Moore, B. Gillespie, and P. Akella, "Cobot architecture," *IEEE Transactions on Robotics and Automation*, vol. 17, no. 4, pp. 377–390, 2001.

[6] J. Funda, R. Taylor, B. Eldridge, S. Gomory, and K. Gruben, "Constrained cartesian motion control for teleoperated surgical robots," *IEEE Transactions on Robotics and Automation*, vol. 12, no. 3, pp. 453–465, 1996.

[7] S. Bowyer, B. Davies, and F. y Baena, "Active constraints/virtual fixtures: A survey," *IEEE Transactions on Robotics*, vol. 30, no. 1, pp. 138–157, 2014.

[8] R. Prada and S. Payandeh, "On study of design and implementation of virtual fixtures," *Virtual reality*, vol. 13, no. 2, pp. 117–129, 2009.

[9] J. Abbott and A. Okamura, "Stable forbidden-region virtual fixtures for bilateral telemanipulation," *Journal of dynamic systems, measurement, and control*, vol. 128, no. 1, pp. 53–64, 2006.

[10] N. Turro and O. Khatib, "Haptically augmented teleoperation," in *Experimental Robotics VII*, D. Rus and S. Singh, Eds. Berlin Heidelberg: Springer, 2001, pp. 1–10.

[11] R. Kikuuwe, N. Takesue, and H. Fujimoto, "A control framework to generate nonenergy-storing virtual fixtures: Use of simulated plasticity," *IEEE Transactions on Robotics*, vol. 24, no. 4, pp. 781–793, 2008.

[12] S. Bowyer and F. y Baena, "Dissipative control for physical human-robot interaction," *IEEE Transactions on Robotics*, vol. 31, no. 6, pp. 1281–1293, 2015.

[13] M. Li, A. Kapoor, and R. Taylor, "A constrained optimization approach to virtual fixtures," in *IEEE/RSJ International Conference on Intelligent Robots and Systems*, Edmonton, Canada, August 2005, pp. 1408–1413.

[14] A. Bettini, P. Marayong, S. Lang, A. Okamura, and G. Hager, "Vision-assisted control for manipulation using virtual fixtures," *IEEE Transactions on Robotics*, vol. 20, no. 6, pp. 953–966, 2004.

[15] R. Castillo-Cruces and J. Wahrburg, "Virtual fixtures with autonomous error compensation for human-robot cooperative tasks," *Robotica*, vol. 28, no. 2, pp. 267–277, 2010.

[16] W. Wannasuphoprasit, B. Gillespie, E. Colgate, and M. Peshkin, "Cobot control," in *IEEE International Conference on Robotics and Automation*, vol. 4, Albuquerque, New Mexico, USA, April 1997, pp. 3571–3576.

[17] B. Bischof, T. Glück, and A. Kugi, "Combined path following and compliance control for fully actuated rigid body systems in 3-d space," *IEEE Transactions on Control Systems Technology*, vol. 25, no. 5, pp. 1750–1760, 2017.

[18] B. Bischof, T. Glück, M. Böck, and A. Kugi, "Path following control for elastic joint robots," *IFAC-PapersOnLine*, vol. 50, no. 1, pp. 4806–4811, 2017.

[19] T. Glück, B. Bischof, and A. Kugi, "Surface following control for fully actuated rigid body systems in three-dimensional euclidean space," *IFAC-PapersOnLine*, vol. 49, no. 18, pp. 594–599, 2016.

[20] R. Gill, D. Kulić, and C. Nielsen, "Spline path following for redundant mechanical systems," *IEEE Transaction on Robotics*, vol. 31, no. 6, pp. 1378–1392, 2015.

[21] C. Nielsen and M. Maggiore, "On local transverse feedback linearization," *SIAM Journal on Control and Optimization*, vol. 47, no. 5, pp. 2227–2250, 2008.

[22] M. Böck and A. Kugi, "Manifold stabilization and path-following control for flat systems with application to a laboratory tower crane," in *IEEE Conference on Decision and Control*, Los Angeles,CA, USA, Dec 2014, pp. 4529–4535.

[23] W.-S. Lu and Q.-H. Meng, "Impedance control with adaptation for robotic manipulators," *IEEE Transactions on Robotics and Automation*, vol. 7, no. 3, pp. 408–415, 1991.

[24] F. Caccavale, C. Natale, B. Siciliano, and L. Villani, "Six-dof impedance control based on angle/axis representations," *IEEE Transactions on Robotics and Automation*, vol. 15, no. 2, pp. 289–300, 1999.

[25] N. Hogan, "Impedance control: An approach to manipulation," *Journal of dynamic systems, measurement, and control*, vol. 107, pp. 1–24, 1985.

[26] B. Siciliano, L. Sciavicco, L. Villani, and G. Oriolo, *Robotics: Modelling, Planning and Control*. London: Springer, 2009.

[27] C. Ott, A. Albu-Schaffer, A. Kugi, and G. Hirzinger, "On the passivity-based impedance control of flexible joint robots," *IEEE Transactions on Robotics*, vol. 24, no. 2, pp. 416–429, 2008.

[28] S. Chiaverini, B. Siciliano, and L. Villani, "A survey of robot interaction control schemes with experimental comparison," *IEEE Transactions on Mechatronics*, vol. 4, no. 3, pp. 273–285, 1999.

[29] S. Bowyer and F. y Baena, "Deformation invariant bounding spheres for dynamic active constraints in surgery," *Proceedings of the Institution of Mechanical Engineers, Part H: Journal of Engineering in Medicine*, vol. 228, no. 4, pp. 350–361, 2014.

[30] J. Swevers, C. Ganseman, B. Tukel, J. De Schutter, and H. V. Brussel, "Optimal robot excitation and identification," *IEEE Transactions on Robotics and Automation*, vol. 13, no. 5, pp. 730–740, 1997.

[31] J. Swevers, W. Verdonck, and J. De Schutter, "Dynamic model identification for industrial robots," *IEEE Control Systems Magazine*, vol. 27, no. 5, pp. 58–71, 2007.

Bernhard Bischof received the Dipl.-Ing. degree in electronics from the UAS Technikum Wien, Vienna, Austria, in 2003. He has been a research assistant with the Automation and Control Institute, TU Wien, Vienna, since 2014. His current research interests include physics-based mathematical modeling and control of mechatronic systems.

Post-print version of the article: B. Bischof, T. Glück, M. Böck, and A. Kugi, "A path/surface following control approach to generate virtual fixtures", *IEEE Transactions on Robotics*, vol. 34, no. 6, pp. 1577–1592, 2018, ISSN: 1552-3098. DOI: 10.1109/TRO.2018.2861913
The content of this post-print version is identical to the published paper but without the publisher's final layout or copy editing.

Tobias Glück received the diploma in engineering cybernetics from the University of Stuttgart, Stuttgart, Germany, in 2007, and the Ph.D. (Dr.techn.) degree in electrical engineering from TU Wien, Vienna, Austria, in 2013. He is currently with the Austrian Institute of Technology, Vienna, Austria. His current research interests include physics-based modeling and control of mechatronic systems.

Martin Böck received the Dipl.-Ing. degree in mechatronics from Johannes Kepler University, Linz, Austria, and the Ph.D. degree in control engineering from Vienna University of Technology (TU Wien), Austria, in 2010 and 2016, respectively. From 2010 to 2017, he was a research assistant with the Automation and Control Institute at TU Wien. His research interests include optimization-based control methods, manifold stabilization, path following control, and differential geometric methods for nonlinear control.

Andreas Kugi (M'94) received the Dipl.-Ing. degree in electrical engineering from TU Graz, Austria, and the Ph.D. degree in control engineering from Johannes Kepler University (JKU), Linz, Austria, in 1992 and 1995, respectively. In 2000, he got the Habilitation in the field of control theory and automatic control at JKU and he was a full professor for system theory and automatic control at Saarland University in Germany from 2002 to 2007. Since June 2007, he is a full professor for complex dynamical systems and head of the Automation and Control Institute at TU Wien, Austria and since 2017, he is also the head of the Center for Vision, Automation & Control at the Austrian Institute of Technology (AIT). His main research interests include the modeling, nonlinear control and optimization of complex dynamical systems, the mechatronic system design, as well as robotics and process automation. He is full member of the Austrian Academy of Sciences and member of the German National Academy of Science and Engineering (acatech).

Post-print version of the article: B. Bischof, T. Glück, M. Böck, and A. Kugi, "A path/surface following control approach to generate virtual fixtures", *IEEE Transactions on Robotics*, vol. 34, no. 6, pp. 1577–1592, 2018, ISSN: 1552-3098. DOI: 10.1109/TRO.2018.2861913
The content of this post-print version is identical to the published paper but without the publisher's final layout or copy editing.